

**EPAC1 activation by cAMP stabilizes CFTR at the membrane by promoting its interaction with NHERF1**

**Summary statement:** Activation of the cAMP sensor EPAC1 leads to stabilization of CFTR at the plasma membrane, through a mechanism that involves the PDZ adaptor NHERF1 and may be used to increase the rescue of mutant CFTR

Miguel J Lobo<sup>1,2</sup>, Margarida D Amaral<sup>1</sup>, Manuela Zaccolo<sup>2</sup>, Carlos M Farinha<sup>1</sup>

<sup>1</sup> University of Lisboa, Faculty of Sciences, BioISI – Biosystems & Integrative Sciences Institute, Campo Grande, 1749-016 Lisboa, Portugal

<sup>2</sup> Department of Physiology, Anatomy & Genetics, University of Oxford, Oxford, OX1 3QX, UK

**Correspondence to:**

Carlos M. Farinha, Departamento de Química e Bioquímica, Faculdade de Ciências da Universidade de Lisboa, Campo Grande, 1749-016 Lisboa, Portugal; Tel.: +351 217500932; e-mail: [cmfarinha@fc.ul.pt](mailto:cmfarinha@fc.ul.pt)

**Running Title:** EPAC1 stabilizes CFTR at the membrane

## **Abstract**

Cyclic AMP (cAMP) activates protein kinase A (PKA) but also the guanine nucleotide exchange factor EPAC1 (exchange protein directly activated by cAMP). While phosphorylation by PKA is known to regulate CFTR channel gating, the protein defective in cystic fibrosis (CF), the contribution of EPAC1 to CFTR regulation remains largely undefined. Here we demonstrate that in human airway epithelial cells cAMP signaling through EPAC1 promotes CFTR stabilization at the PM by attenuating its endocytosis, independently of PKA activation. EPAC1 and CFTR co-localize and interact through protein adaptor NHERF1. This interaction is promoted by EPAC1 activation triggering its translocation to the PM and binding to NHERF1. Our findings identify a novel CFTR interacting protein and demonstrate that cAMP activates CFTR through two different but complementary pathways – the well-known PKA-dependent channel gating and a novel regulatory mechanism of endocytosis involving EPAC1. The latter may constitute a novel therapeutic target for CF.

## **Keywords**

CFTR/ cAMP/ EPAC1/ membrane stability/ protein trafficking

## **Introduction**

The cystic fibrosis transmembrane conductance regulator (CFTR) is an integral membrane protein of the ATP-binding cassette (ABC) transporter family that functions as a cAMP-activated Cl<sup>-</sup> ion channel at the apical membrane of several fluid-transporting epithelia (Riordan, 2008) including the airways, where it has an active role in controlling airway surface liquid homeostasis through promotion of mucociliary clearance (Boucher, 2004). CFTR possesses two transmembrane domains (TMD1/2), two nucleotide binding domains (NBD1/2), that bind and hydrolyse ATP regulating the gating of the channel, and a regulatory domain (RD) with multiple phosphorylation sites (Riordan, 2008). Cl<sup>-</sup> secretion through CFTR depends on the net balance of channel density at the cell surface and the activity of each individual channel (Cihil et al., 2012). CFTR dysfunction leads to cystic fibrosis (CF), the most common life-threatening recessive disorder in Caucasians.

Steady-state levels of CFTR at the plasma membrane (PM) rely on its biosynthetic processing, early and late secretory trafficking as well as on its endocytic uptake, the latest being followed either by recycling to the PM or lysosomal degradation (Farinha et al., 2013b; Riordan, 2008). As CFTR internalization at the cell surface is a rapid process compared to CFTR biosynthesis and anterograde trafficking, the recycling of internalized channels is considered to be a key process for sustaining a functional pool of CFTR at the PM (Farinha et al., 2013b; Haggie et al., 2006). Membrane trafficking of CFTR is stringently regulated by several protein interactors that bind to its C-terminus. Among these, the PDZ adaptor protein Na<sup>+</sup>/H<sup>+</sup>-exchanger regulatory factor isoform-1 (NHERF-1, also known as EBP50, ezrin-binding protein with 50kDa) is responsible for anchoring PM CFTR to the actin cytoskeleton (Wang et al., 1998). NHERF-1 links CFTR to the ezrin/radixin/moesin (ERM) family protein ezrin and locks the channel in an immobile and actin-tethered complex that prevents its endocytosis (Reczek et al., 1997; Sun et al.,

2000a). Therefore, CFTR surface anchoring and retention may constitute a major target pathway for CF pharmacotherapy (Farinha et al., 2013b; Young et al., 2009) especially considering that the rescued form of the most common CF-causing CFTR mutant (F508del-CFTR) still exhibits a decreased stability at the PM (Amaral and Farinha, 2013).

CFTR channel gating at the PM involves cAMP-activation of protein kinase A (PKA), that phosphorylates CFTR regulatory domain (RD) (Sheppard and Welsh, 1999). This PKA-mediated activation of CFTR relies on a local pool of cAMP near the membrane that is regulated by the integrity of the actin cytoskeleton (Favia et al., 2010; Monterisi et al., 2012). Although it is well established that cAMP plays a crucial role in CFTR channel gating through PKA, this kinase is not the only cAMP effector within the cell and the other cAMP-dependent signaling pathways may also impact on CFTR.

EPAC1, an exchange protein directly activated by cAMP, functions as a guanine nucleotide exchange factor (GEFs) for both Rap1 and Rap2 (de Rooij et al., 2000) and is able to suppress the oncogenic transformation of cells by Ras (Gloerich and Bos, 2010). In response to cAMP, EPAC1 is targeted to the PM where it tethers to phosphatidylic acid or to phosphorylated ERM proteins to induce its downstream effectors (Schmidt et al., 2013).

Regulation of CFTR channel gating through EPAC1 activation has been addressed and is apparently tissue-specific. One study proposes a role for EPAC1 in intestinal chloride secretion through a PKA-independent mechanism not involving CFTR (Hoque et al., 2010) but a more recent one postulates that, in bronchial cells, EPAC1 promotes amplification of the cAMP signal evoked by H<sub>2</sub>O<sub>2</sub> through a mechanism that involves PKA (Ivonne et al., 2015). However, EPAC1 localization at the PM, where it is potentially exposed to the same pool of increased subcortical cAMP that induces PKA-mediated activation of CFTR, and its ability to promote cortical cytoskeleton stabilization (Kooistra et al., 2005) suggest that

EPAC1 might be involved in the regulation of CFTR membrane stability and/or PM anchoring. Although a more direct connection between CFTR and EPAC1 was never reported, this cAMP effector is involved in the regulation of cell-to-cell and cell-matrix adhesion, cytoskeleton rearrangements and cell polarization, processes which are described to affect CFTR regulation and to be dysregulated in CF (Monterisi et al., 2012). Herein, we explored the interaction between CFTR and EPAC1 and evaluated the impact of this cAMP effector on CFTR biogenesis, trafficking and PM anchoring. We show that EPAC1 and CFTR co-localize and interact through the protein adaptor NHERF1 and that EPAC1 activation promotes the NHERF1-CFTR interaction stabilizing the latter at the PM. Altogether, these results reveal a novel CFTR interacting protein that links cAMP signaling to Cystic Fibrosis modulation via a previously unreported mechanism. Furthermore, EPAC1 can be used as a novel therapeutic target to stabilize mutant CFTR at the PM.

## Results

### *Cyclic AMP increases CFTR levels at the plasma membrane*

To address whether an increase in intracellular cAMP affects CFTR levels at the PM, CFBE cells expressing wt-CFTR (CFBE-wt) were treated with increasing concentrations of forskolin (Fsk) to induce adenylate cyclase activation and hence cAMP. Levels of CFTR at the PM were assessed by cell surface biotinylation, followed by streptavidin pull-down and CFTR detection by Western blot (*Figure 1A and B*). Results show an increase in CFTR PM levels with increased Fsk concentrations, detectable from 1  $\mu$ M and higher concentrations and with peaks observed at 10  $\mu$ M and 25  $\mu$ M (*Figure 1B*). This however, does not correspond to an increase in total CFTR levels or in its steady-state processing levels, as evidenced by similar levels of mature CFTR (band C) over total CFTR across these treatments (*Figure 1A*, middle panel – CFTR WCL). 50  $\mu$ M is the saturating concentration of Fsk since there is no further increase in CFTR PM levels when this Fsk concentration is combined with 100  $\mu$ M of the phosphodiesterase inhibitor IBMX (*Figure 1C*).

### *Increase of CFTR at the plasma membrane occurs through EPAC1 activation*

Since increase of subcortical cAMP levels has been known for long to activate PKA, thus promoting CFTR function, we assessed whether the observed increase in CFTR PM levels was also dependent on PKA activation. To test this hypothesis cell surface levels of CFTR were assessed in CFBE-wt cells under treatment with the cAMP analogue 6-Bnz-cAMP-AM that selectively activates PKA (Christensen et al., 2003) or transfected with the PKA inhibitor (PKI) (Tkachenko et al., 2011). Treatment with this agonist (*Figure 1D and E*) or the inhibitor (*Figure 1F and G*) did not affect CFTR PM levels. To further clarify the mechanism for the observed increase in CFTR PM levels, we then assessed the effect of

activation of EPAC1. To this end, we used a cAMP analogue that selectively activates EPAC1 (8-(4-Chlorophenylthio)-2'-O-methyladenosine-3',5'-cyclic monophosphate acetoxymethyl ester, hereafter named 007-AM) (Christensen et al., 2003; Schwede et al., 2015).

Firstly, to assess the EPAC1 selectivity of this compound in CFBE cells, we measured sensitized emission from two different FRET reporters: one based on EPAC1 (camps) (DiPilato et al., 2004; Ponsioen et al., 2004) and another based on a PKA substrate (AKAR4) (Liu et al., 2011). The 007-AM agonist induced a large FRET change for camps but only a minor FRET change in AKAR4 (*Figure S1A-C*), indicating that 007-AM is an EPAC1-specific agonist in CFBE cells. Conversely, the PKA agonist 6-Bnz-cAMP-AM is able to activate only the AKAR4 but not the camps sensor (*Figure S1D-F*). Additionally, PKA inhibition with PKI precludes activation of the AKAR4 but not of the camps sensor (*Figure S1G and H*). Specificity of EPAC1 activation with 007-AM was confirmed by assessing the activation of Rap1 using both the Raichu-Rap FRET sensor (Mochizuki et al., 2001) and a Rap activity assay (Franke et al., 1997). We observed that, after treatment with 007-AM, CFBE-wt cells show a FRET increase at the PM for this sensor (*Figure S1I and J*) and also to a trend of increase in active Rap1A levels (*Figure S1K and L*).

We then, assessed the effect of 007-AM treatment on CFTR PM levels. We observed an increase in CFTR-PM levels after stimulation with 1 $\mu$ M 007-AM for 2h (*Figure 1D and E*) and that this time point corresponds to its maximal effect (*Figure S2A and B*). To further validate the role of EPAC1 in regulating CFTR PM levels, we assessed the effect of reducing its levels by siRNA. EPAC1 siRNA-specific knockdown decreased its total levels by 50.4% compared to control siRNA and, in agreement with our results with the selective EPAC1 activator, this decrease in EPAC1 levels correlated with a 82.5% decrease in the levels of PM CFTR compared to control (*Figure 1H, I and J*). Interestingly, either treatment

with 007-AM or transfection with a specific siRNA targeting EPAC1 did not affect neither total levels of CFTR nor its processing at steady-state (mature CFTR - band C - over total CFTR) in these cells (*Figure 1D and E*, WCL). These data suggest that the observed effects are not caused by changes in CFTR synthesis, turnover or ER-to-Golgi trafficking but rather result from either enhanced channel delivery from the trans-Golgi network (TGN) to the PM or its increased retention at the PM, i.e., decreased endocytosis or increased recycling.

To assess whether the increased levels of CFTR at the PM correspond also to an increase in overall function, we tested wt-CFTR channel activity in CFBE cells by iodide efflux. We observed higher levels of CFTR activity in cells treated with 1 $\mu$ M 007-AM or 25 $\mu$ M Fsk for 2h, as they exhibited a decreased iodide concentration that remained inside the cells (56.9% $\pm$ 13.7 or 58.3% $\pm$ 18.6, respectively) in comparison to DMSO-treated cells (*Figure 1K*). Interestingly, pre-incubation of the cells with the PKA agonist 6-Bnz-cAMP-AM for 2h did not lead to an increased CFTR activity and the combined effect of this agonist with 007AM is equivalent to 007-AM alone (54.4% $\pm$ 14.8 or 56.9% $\pm$ 13.7, respectively). This result confirms that EPAC1 activation increases the levels of functional CFTR at the PM in CFBE-wt cells.

#### *EPAC1 activation reduces CFTR endocytosis*

Since treatment with either 007-AM or EPAC1-specific siRNA do not significantly impact on total CFTR levels (see above), we aimed at dissecting how EPAC1 activation increases CFTR PM levels. First, we performed a modified cell surface biotinylation assay to determine CFTR endocytosis rate. Results show that EPAC1 activation with 007-AM decreases CFTR internalization over time (*Figure 2A and B*). These results suggest that

EPAC1 promotes CFTR stability at the PM by attenuating its endocytosis. To further understand this mechanism, we assessed the effect of blocking endocytic pathways using a potent inhibitor of dynamin-dependent endocytic pathways - dynasore - thus blocking CFTR internalization (Macia et al., 2006; Young et al., 2009) and again assessed CFTR PM levels by cell surface biotinylation. Under conditions that inhibit endocytosis, this approach assesses CFTR delivery to the cell surface. Results show that treatment with dynasore promotes an overall increase of 3.4-fold in the levels of CFTR at the PM. However, there was no statistically significant difference between DMSO, 007-AM or Fsk treatments in combination with dynasore (*Figure 2C and D*), suggesting that EPAC1 activation does not interfere with CFTR delivery from TGN to the PM but rather with its retention at the PM.

To determine whether the observed effects upon CFTR internalization are due to either decreased endocytosis or increased recycling, we then performed a modified cell surface biotinylation protocol to assess CFTR recycling rate and thus distinguish between these two hypotheses. We observed that EPAC1 activation with 007-AM did not significantly alter CFTR recycling rates at 2.5, 5 and 10 min in comparison to DMSO treatment (*Figure 2E and F*). Altogether, these results indicate that EPAC1 promotes CFTR stability at the PM through attenuation of its endocytosis.

To assess the specificity of this effect of EPAC1 activation on CFTR trafficking, we tested the effect of 007-AM on another cell surface protein, EGFR (Epidermal Growth Factor Receptor). Results from endocytosis assays show that EPAC1 activation with 007-AM did not significantly change neither EGFR PM levels nor its endocytosis rate at 10 min in comparison to DMSO treatment (*Figure S2C-E*), suggesting that the EPAC1-mediated CFTR stabilization is not a broad mechanism involved in the general regulation of PM proteins.

*Activation of EPAC1 promotes its translocation to the PM and co-localization with CFTR*

To characterize the mechanism through which EPAC1 stabilizes CFTR at the PM, we characterized the cellular localization of EPAC1 and CFTR upon EPAC1 activation.

To this end, we first assessed the effect of 007-AM on EPAC1 localization by fluorescence confocal microscopy. CFBE parental, -wt or -F508del cells were transfected with GFP-EPAC1. EPAC1 is mainly localized in the cytosol and around the nucleus under basal conditions and it translocates to the PM after activation with 1 $\mu$ M 007-AM. This effect was detected both in CFBE and HEK293T cells, the latter cells being used as a control for which EPAC1 translocation to the PM after 1 $\mu$ M 007-AM treatment was previously reported (Consonni et al., 2012; Gloerich et al., 2010; Ponsioen et al., 2009) (*Figure 3A-C and Figure S3*). The translocation occurs within the first 3 min of incubation with 007-AM and does not depend on the presence of CFTR (as it is detected in all 3 types of cells). This relocation of activated EPAC1 suggests that this protein and CFTR may co-localize or even interact.

To assess the co-localization between CFTR and EPAC1, CFBE parental cells were co-transfected with mCherry-CFTR (wt or F508del) and GFP-EPAC1 and live-cell imaging was performed (*Figure 3D and E*). As expected, wt-CFTR localizes at the PM while F508del-CFTR localization is perinuclear. In CFBE-wt/F508del cells under pre-stimulus conditions, EPAC1 localizes to the cytosol and translocates to the PM after activation with 1 $\mu$ M 007-AM. Thus, treatment with this cAMP analogue increases co-localization between CFTR and EPAC1 as assessed by Pearson's coefficient (*Figure 3F*) in CFBE-wt cells, while it decreases this co-localization in CFBE-F508del cells.

*CFTR and EPAC1 co-immunoprecipitate*

To assess whether the observed co-localization corresponds to the presence of CFTR and EPAC1 in the same protein complexes, co-immunoprecipitation experiments were performed in CFBE and A549 cells (*Figure 4*).

Results show that GFP-EPAC1 co-immunoprecipitates with mCherry-wt-CFTR under basal conditions in CFBE parental cells transiently transfected with both constructs, suggesting that although the degree of co-localization under these conditions was close to 0.5, these proteins can still interact with each other (*Figure 4A*). The same experiment was performed in A549 or CFBE cells expressing mCherry-wt- or F508del-CFTR (*Figure 4B and D*) and endogenously expressed EPAC1. Besides confirming that EPAC1 co-immunoprecipitates with wt-CFTR, results from this experiment also produced the same observation for F508del-CFTR. This may indicate that EPAC1 can interact with CFTR in the early stages of its trafficking, i.e. even if the protein is not at the PM. Co-immunoprecipitation experiments were repeated in the same cell lines under EPAC1 activation with 1 $\mu$ M 007-AM. The treatment increases the association between CFTR (wt or F508del) and EPAC1 (*Figure 4B-F*), suggesting that, at least for wt-CFTR, the interaction is promoted when EPAC1 is active and near the PM. After being activated, EPAC1 translocates from the cytosol and perinuclear region to the PM vicinity, which may facilitate the interaction with CFTR. The effect of 007-AM in promoting the interaction between EPAC1 and CFTR appears to be more pronounced for wt than for F508del-CFTR (*Figure 4E and F*). Taken together, the co-immunoprecipitation between CFTR and constitutive EPAC1 and their PM distribution in human airway epithelial cells indicates that CFTR and EPAC1 are present in the same protein complexes.

*EPAC1 interacts with CFTR through NHERF1*

Since EPAC1 has been previously reported to either interact or regulate processes dependent on NHERF1 and ezrin (Gloerich and Bos, 2010) – both proteins also known to interact with CFTR (Farinha et al., 2013b), we hypothesized that CFTR and EPAC1 may interact through one of these scaffold proteins. In fact, EPAC1 (UniProtKB accession numbers O95398) does not contain a PDZ domain within its sequence, supporting the need of an adaptor protein between CFTR and EPAC1.

To test this hypothesis, we assessed CFTR interaction with EPAC1 under down-regulation of either ezrin or NHERF1. This was performed in CFBE-wt cells transiently transfected with specific siRNAs (*Figure 5A-C*) and Calu3 cells stably transduced with lentiviral particles expressing shRNAs against each protein (*Figure 5D-F*). As observed, NHERF1, but not ezrin, knockdown abolishes the interaction between EPAC1 and CFTR. Results in Calu-3 show that the above-described CFTR-EPAC1 interaction (*Figure 4*) also occurs when both proteins are endogenously expressed (*Figure 5D*). These results suggest that NHERF1, but not ezrin, mediates EPAC1-CFTR interaction.

As the disruption of the CFTR-EPAC1 interaction may also result from a change in the sub-cellular localization of EPAC1 when NHERF1 levels are decreased, we performed fluorescence live-cell imaging in Calu3 cells transfected with GFP-EPAC1 (*Figure S3A and B*). Our results show that neither EPAC1 sub-cellular localization nor its translocation to the PM after 1 $\mu$ M 007-AM treatment were affected by either ezrin or NHERF1 knockdown.

Additionally, to further characterize the mechanism of CFTR increase at the PM under EPAC1 activation, we used cell surface biotinylation to assess the levels of PM CFTR after 007-AM in cells where either NHERF1 or ezrin were knocked down. Results show that NHERF-1, but not ezrin, knockdown prevents the stabilization of CFTR at the PM after

EPAC1 activation (*Figure 5G and H*). These observations are in agreement with the hypothesis that EPAC1-CFTR interaction is mediated by NHERF1.

#### *EPAC1 interacts with NHERF1*

To further dissect the role of NHERF1 in the stabilization of CFTR at the PM by EPAC1, we used co-immunoprecipitation to assess if EPAC1 and NHERF1 interact in both CFBE and HEK293T cells (*Figure 6*). As observed, EPAC1 and NHERF1 co-immunoprecipitate and EPAC1 activation also promotes the interaction between these proteins (*Figure 6C and D*), strengthening our hypothesis that CFTR-EPAC1 interaction is mediated by NHERF1.

To better characterize the EPAC1-NHERF1 interaction, we aimed at identifying specific domains involved in the interaction. We observed that the interaction is disrupted after deletion of the PDZ1 domain of NHERF1, suggesting that this may be the domain mediating that interaction (*Figure S4A*). On the other hand, deletion of the N-terminal region of EPAC1 impaired the interaction between EPAC1 and NHERF1 (*Figure S4B*) suggesting that it may be mediated by this region. Overall, the interaction seems to be mediated by NHERF1 PDZ1 domain and EPAC1 N-terminus.

#### *EPAC1 activation is additive to F508del-CFTR rescue with VX-809*

Lastly, we assessed whether EPAC1 activation is also able to increase the rescue of F508del-CFTR by the recently FDA-approved drug VX-809. To this end, CFBE-F508del cells were incubated with 3 $\mu$ M VX-809 to promote the rescue of the mutant protein combined with 1 $\mu$ M 007-AM to activate EPAC1 (*Figure 7A and B*). Levels of mature and

immature CFTR were assessed by WB. Results show that the combined effects of VX-809 and 007-AM increase F508del-CFTR processing levels from 11/13% in VX-809 treated cells (for 24/48h) to 17/19% in cells treated with both compounds. Additionally, we assessed the effect of EPAC1 activation on the channel activity of VX-809-rescued F508del-CFTR in CFBE cells. We detected a lower amount of iodide remaining inside the cells (20% decrease relative to cells treated only with VX-809), i.e. higher levels of CFTR activity, in cells treated with both compounds (*Figure 7C*). These findings indicate that targeting CFTR membrane stability through EPAC1 activation may be an approach to be used in combination with corrector treatment.

## Discussion

Ion transport through CFTR is stimulated when levels of cAMP in the subcortical compartment are increased leading to PKA activation, thus triggering CFTR phosphorylation and channel opening. However, besides PKA, EPAC1, an exchange protein directly activated by cAMP, is another more recently discovered cAMP effector (Gloerich and Bos, 2010). Here we describe a PKA-independent cellular mechanism that links cAMP to CFTR regulation in CF bronchial epithelial cells.

Our data demonstrate that an increase in cAMP levels promotes CFTR stability at the PM (*Figure 1*). A maximal effect is observed under stimulation with 10-25  $\mu\text{M}$  Fsk whereas no significant increase in CFTR PM levels is observed for the range of Fsk concentrations (0.1-1.0  $\mu\text{M}$ ) reported to maximally induce CFTR chloride currents in CFBE-wt cells (Bebok et al., 2005). This suggests that cAMP signaling may regulate CFTR across a broad range of concentrations. PKA-mediated cAMP signals regulate CFTR function at lower cAMP concentrations, while EPAC1-dependent regulation works for higher cAMP levels. This is in agreement with the fact that cAMP exhibits a lower affinity for EPAC1 ( $K_d$  2.8  $\mu\text{M}$ ) than for PKA ( $K_d$  0.1-1.0  $\mu\text{M}$ ) (Christensen et al., 2003). Moreover, PKA effect on CFTR function is fast but short in time while EPAC1-mediated effect occurs at later and for higher levels of cAMP. Thus, this cAMP-dependent dual control of CFTR allows for a temporal and spatial precise control of chloride secretion. In fact, our observations are in agreement with published work suggesting that treatment with Fsk/IBMX could enhance CFTR membrane trafficking (Chang et al., 2002). Here we demonstrate that this effect on CFTR relies on cAMP-dependent activation of EPAC1 and does not involve PKA. This EPAC1-dependent effect was further confirmed through EPAC1 knockdown with siRNA that lead to a decrease in PM levels of CFTR (*Figure 1*). This effect leads to an increase in CFTR function (*Figure 1*), an observation that is in agreement with a recent report according to

which EPAC1 is involved in signal amplification occurring during CFTR activation by H<sub>2</sub>O<sub>2</sub> (Ivonne et al., 2015). Our study now shows that in bronchial cells this increase likely occurs through membrane stabilization of CFTR.

Moreover, we found that EPAC1 activation promotes an increase in CFTR levels at the PM, through a decrease in its endocytosis (*Figure 2*). Interestingly we also show that this stabilization effect is not observed for the unrelated membrane protein EGFR, suggesting that this is not a general regulation mechanism nonspecifically affecting any membrane protein (*Figure S2C-E*). As we detected no changes in either delivery to the cell surface or endocytic recycling, the observed effect may impair recognition of endocytic signals or simply potentiate its binding to NHERF1, an adaptor protein essential for CFTR anchoring to the actin cytoskeleton (Favia et al., 2010; Loureiro et al., 2015).

Several approaches support the effect of EPAC1 on CFTR regulation. First, we evaluated the effect of 007-AM treatment on EPAC1 sub-cellular localization, tertiary structure, and activity (*Figure 3, Figure S1 and Figure S3*) and confirmed that this molecule is an EPAC1-specific agonist and validated the concentration of this compound used for this study (1 $\mu$ M) as correct to promote maximal EPAC1 activation in this cellular model.

EPAC1 translocation to the PM after 007-AM treatment was observed in CFBE cells and found to be independent of CFTR (*Figure 3*). In fact, this translocation occurs in CFBE-wt, CFBE-F508del and parental CFBE cells. This is in agreement with previous reports showing that EPAC1 translocates to the PM, a process dependent on its structural change and binding to phosphatidic acid or ERM proteins (Consonni et al., 2012; Gloerich et al., 2010). EPAC1 translocation to the PM, together with the observed stabilization of CFTR at the PM under 007-AM, suggested that EPAC1 and CFTR may co-localize or interact with each other, mainly under 007-AM treatment.

In fact, our results show that EPAC1 co-localizes with both wt- or F508del-CFTR in CFBE cells without stimulus or under 007-AM treatment (*Figure 3*). Additionally, the two proteins co-immunoprecipitate in CFBE, A549 and Calu3 cells (*Figure 4 and 5*). The fact that EPAC1 interaction is also detected with F508del-CFTR suggests that this interaction may also occur at the early stages of CFTR trafficking and thus before CFTR reaches the PM, despite being stronger when EPAC1 is active and mostly located at the PM. As CFTR/EPAC1 co-immunoprecipitation is detected in the absence of EPAC1 activation with 007-AM, endogenous levels of cAMP may be enough to promote some EPAC1 activation and thus its interaction with CFTR. Nevertheless, our data also suggest that active EPAC1 has an increased association with CFTR compared to inactive EPAC1.

This increased CFTR-EPAC1 interaction under EPAC1 activation may result from different molecular events that are not mutually exclusive: 1) EPAC1 undergoes a conformational change; 2) EPAC1 translocates to the PM; or/and 3) EPAC1 becomes catalytically active. After being activated, EPAC1 translocates from the cytosol and perinuclear region to the PM vicinity, which may facilitate the interaction with CFTR, namely with wt-CFTR. This may explain why the promotion of the interaction between EPAC1 and wt-CFTR by 007-AM is stronger than that of F508del-CFTR. Moreover, EPAC1 activation does not affect the band C/band B ratio, a readout for the proportion of CFTR that has been processed, thus indicating that its role in the early stages of CFTR biogenesis is less relevant.

On the other hand, NHERF1, but not ezrin, knockdown (through siRNA or shRNA transfection) prevented CFTR-EPAC1 interaction without disrupting EPAC1 sub-cellular localization (*Figure 5 and Figure S3A and B*), suggesting that EPAC1 may interact with CFTR through the NHERF1 mediator. The fact that EPAC1 does not contain a PDZ domain within its sequence supports the need of an adaptor protein for the CFTR-EPAC1 interaction to occur. Our data suggest that such a role is played by NHERF1, that

generally functions as a protein adaptor highly expressed in epithelial tissues (Voltz et al., 2001). Furthermore, our data clearly show that EPAC1 co-immunoprecipitates with NHERF1, being this interaction also potentiated under EPAC1 activation (*Figure 6 and Figure S4*).

Our results further clarify that the interaction between EPAC1 and NHERF1 may be mediated by NHERF1 PDZ1 domain. In the absence of ezrin, NHERF1 PDZ2 domain is inhibited. Binding of ezrin to NHERF1 promotes a conformational change exposing the PDZ2 domain (Morales et al., 2007). If the binding of EPAC1 to NHERF1 were PDZ2-mediated, then the absence of ezrin would abolish this interaction – but our results show that ezrin knockdown does not affect CFTR-EPAC1 interaction. Therefore, according to our data, EPAC1 binds CFTR through NHERF1, an observation that is in agreement with the previously binding of PKA to CFTR through ezrin.

It has also been suggested that ezrin can positively regulate the cooperative binding of NHERF to CFTR C-terminus (Li et al., 2005). As a result of ezrin binding, a specific ternary complex (CFTR)<sub>2</sub>-NHERF-Ezrin with 2:1:1 stoichiometry is formed, in which two CFTR molecules are anchored to NHERF (Li et al., 2005). Nevertheless, one possibility is that NHERF1 interacts simultaneously with CFTR and EPAC1 through its PDZ domains, and with ezrin through its carboxyl terminus (the latter may also tether PKA). Moreover, ezrin is a kinase-anchoring protein, bringing PKA, phosphatases, phosphodiesterases and other signaling proteins to the vicinity of CFTR (Monterisi et al., 2012; Sun et al., 2000b). The generation of a macromolecular complex involving cytoskeleton proteins may play a key role in fine-tuning the regulation of CFTR stability and function (Monterisi et al., 2013). In fact, our data support a model of a macromolecular complex where CFTR, EPAC1 and NHERF1 interact, the latter acting as a mediator, possibly with proteins like ezrin (*Figure 7*).

Interestingly, modulation of such macromolecular complex (and its stabilizing effect upon PM CFTR) can be used to improve the functional rescue of F508del-CFTR (*Figure 7*). Recent evidence shows that the correction of F508del-CFTR trafficking defect by VX-809 (Van Goor et al., 2011) has modest therapeutic efficacy (Clancy et al., 2012; Wainwright et al., 2015), suggesting that a combinatorial approach is needed to achieve correction levels that translate in clinical benefit (Amaral and Farinha, 2013; Farinha et al., 2013a). Our results show that the combined effect of VX-809 and 007-AM improves F508del-CFTR rescue relatively to VX-809 by an additional 6% (from 11% to 17%). Altogether, these results enforce the hypothesis that modulation of the EPAC1 pathway may constitute an additional strategy for the functional correction of F508del-CFTR. Interestingly, this effect seems to be specific of respiratory epithelia, as it was previously shown that EPAC1 also mediates chloride secretion in the intestine but without the involvement of CFTR (Hoque et al., 2010). Thus, EPAC1 activation is a putative novel target in the organ that is responsible for most of the morbidity and mortality associated with CF. These observations are in agreement with previous use of compounds that elevate intracellular levels of cAMP as therapeutic options in respiratory diseases such as asthma and COPD (Schmidt et al., 2013). Being EPAC1, as well as its effectors Rap1 and Rap2, expressed in human bronchial epithelial cells, this may be also a mechanism to regulate epithelial integrity in diseased cells. In fact, EPAC1 is involved in the inhibition of cell proliferation and is thus related to a more differentiated phenotype (Roscioni et al., 2009). Interestingly, EPAC1, whose expression in the adult lung is dominant over that of EPAC2 (Ulucan et al., 2007), also interacts with TGF- $\beta$ , a pro-inflammatory cytokine that is increased in CF patients. This interaction leads to the subsequent inhibition of Smad-dependent TGF- $\beta$  signaling (Conrotto et al., 2007). These observations further strengthen the relevance of EPAC1 in the context of CFTR trafficking and in the overall context of the normal vs CF cell.

In this study we unveiled that cAMP signaling promotes CFTR PM stabilization through EPAC1 activation. These findings demonstrate the existence of a novel mechanism of CFTR regulation by cAMP. In addition to PKA-mediated activation of chloride transport, operating at lower concentrations of cAMP, we identified a novel mechanism through which higher levels of cAMP activate EPAC1 to promote its interaction with NHERF1 and thus stabilizing CFTR at the PM by decreasing its endocytosis rate. This work constitutes an important characterization of a new CFTR interacting protein that links cAMP to Cystic Fibrosis modulation in a previously unreported mechanism.

## Materials and methods

### *Plasmid constructs*

The following plasmids were used: GFP-EPAC1, GFP- $\Delta$ 49-EPAC1 and GFP- $\Delta$ 148-EPAC1, lacking the first 49 or 148 amino acids (Gloerich et al., 2010); GFP-NHERF1, NHERF1-GFP, Myc-NHERF1, GFP-PDZ2-ERM (lacks PDZ1 domain), GFP-ERM (lacks both PDZ1 and 2 domains) (Castellani et al., 2012; Loureiro et al., 2015); Raichu sensor (Nakamura et al., 2006), with the Rap1 sequence between YFP and CFP; pGEX-RalGDS-RBDGST plasmid (Franke et al., 1997); mCherry and PKI-mCherry (Lefkimmiatis et al., 2013).

### *Cell lines and cell transfection*

Cystic Fibrosis Bronchial Epithelial (CFBE41o-) cells (CFBE), stably overexpressing either wt- or F508del-CFTR (CFBE-wt/CFBE-F508del)(Bebok et al., 2005) or without expressing CFTR (parental CFBE)(Gruenert et al., 1995), A549 cells overexpressing mCherry-wt- or mCherry-F508del-CFTR (Almaca et al., 2011) and Calu3 cells (Calu3-wt) (Fogh et al., 1977) were cultured as described. Calu-3 cells transduced expressing a control (Calu3 shControl), ezrin (Calu3 shEzrin) or NHERF1 shRNA (Calu3 shNHERF1) were generated in this work (see below) and cultured with puromycin (5 $\mu$ g/mL). Human Embryonic Kidney (HEK293T) cells were cultured in DMEM supplemented with 10% (v/v) FBS. Cells were transiently transfected with plasmid DNA or siRNA using Lipofectamine2000 (Life Technologies) and analyzed 24 or 48h later. All cells were tested for contamination, including mycoplasma contamination.

*Antibodies and reagents*

The following antibodies were used as recommended by the manufacturers: anti- $\alpha$ -tubulin (Sigma Aldrich, T5168), anti- $\beta$ -tubulin (SCBT, sc-9104), anti-calnexin (BD Biosciences, 610523), anti-CFTR (CF Foundation, 596), anti-EPAC1 (Aviva, ARP52140\_P050), anti-ezrin (BD Biosciences, 610602), anti-GAPDH (SCBT, sc-166574), anti-GFP (SCBT, sc-9996), anti-myc (SCBT, sc-789), anti-NHERF1 (BD Biosciences, 611160), anti-Poli-Ub (BIOMOL, PW8805), anti-Rap1A (SCBT, sc-1482) and horseradish peroxidase-conjugated goat anti-mouse/-rabbit secondary antibodies (BioRad; dilution 1:3000). All primary antibodies were used at 1:1000 dilution except anti-CFTR (1:3000) and anti-Rap1A (1:500). The following reagents were used: 8-pCPT-2'-O-Me-cAMP-AM (007-AM) (BioLog), VX-809 (Selleckchem), Forskolin, IBMX (Sigma-Aldrich) and H89 (Enzo Life Sciences). The following siRNAs were used: Silencer® Select Negative Control No. 2 siRNA and RAPGEF3 (Life Technologies, 4390846 and 4392420), siGENOME SMART pool non-targeting siRNA, human EZR and human SLC9A3R1 (Thermo Scientific, D-001206-13, EG:7430 and EG:9368, respectively).

*Lentivirus infection*

To produce lentiviral particles containing specific shRNAs, HEK293T cells were transiently transfected with the packaging (pCMV-dR8.74psPAX2), envelop (pMD2.G) and hairpin-pLKO.1 vector (control, SHC001; NHERF1, SHCLND SLC9A3R1; Ezrin, SHCLND EZR; Sigma-Aldrich, St.Louis, MO) plasmids using X-tremeGENE9 DNA transfection reagent (Sigma-Aldrich). Medium was removed after 18h incubation at 37°C and replaced with high-BSA growth media (DMEM supplemented with 10% (v/v) iFBS (inactivated FBS), 1.1g/100mL BSA (Bovine serum albumin) and Pen/Strep). The next day, the medium was

collected and stored at -20°C. The cells were incubated again with high-BSA growth medium and harvested again 24h later.

For transduction, Calu3-wt cells were washed with HBSS. EMEM supplemented with 10% (v/v) FBS, polybrene (8µg/mL) and 5-20% (v/v) lentivirus-containing medium was added. and incubated at 37°C for 24h. Medium was then replaced by EMEM supplemented with 10% (v/v) FBS and puromycin (5µg/mL) and this was repeated for, at least, 5 consecutive days.

#### *Western blotting*

Cells were lysed and extracts analyzed as described previously (Farinha et al., 2002). Signal was developed with ImmunStar Western C (BioRad, Hercules, CA) or ECL Substrate (Thermo Scientific). Detection was performed with the Chemidoc XRS+ analyser (BioRad) or using Compact X4 Automatic Processor (Xograph). Quantification was performed using the Image Lab software (BioRad) or ImageJ (<http://imagej.nih.gov/ij/>).

#### *Immunoprecipitation*

Cells were lysed with PD buffer (50mM Tris-HCl, 0.1M NaCl, 1% (v/v) NP40, 10% (v/v) glycerol, pH 7.5) supplemented with protease inhibitor cocktail (Roche) at 4°C and collected with a scraper. Lysate was cleared by centrifugation and the supernatant was pre-cleared through incubation with Protein-G agarose beads (Invitrogen). After that, the supernatant was incubated overnight with the appropriate antibody at 4°C. For mCherry and myc pull-down, anti-RFP antibody-linked beads (Chromotek – Planegg-Martinsried, Germany – RFP-Trap\_A sta-20) and anti-c-Myc antibody-linked beads (Sigma, A7470),

respectively, or untagged beads (Chromotek bab-20), as a control, were used. Beads were washed 3x with wash buffer (Tris-HCl 0.1M, NaCl 0.3M, Triton X-100 1% (v/v), pH 7.5) followed by elution with 1x sample buffer, separation on SDS-PAGE gels and analysis by Western Blot.

#### *Biochemical Determination of Plasma Membrane CFTR*

The determination of PM CFTR was performed by cell surface biotinylation using membrane impermeable EZ-Link™ Sulfo-NHS-SS-Biotin (Pierce Chemical Co., Grand Island, NY), followed by lysis in 25 mM HEPES, pH 8.0, 1% (v/v) Triton, 10% (v/v) glycerol, and Protease Inhibitor Cocktail (Roche), as described (Moyer et al., 1998). Biotinylated proteins were isolated with streptavidin-agarose beads, eluted with sample buffer and separated by SDS-PAGE.

#### *Endocytic and Recycling Assays*

Endocytic and recycling assays were performed as described (Cihil et al., 2012; Swiatecka-Urban et al., 2002). For both assays, PM proteins were first biotinylated at 4 °C using membrane impermeable and cleavable EZ-Link™ Sulfo- NHS-SS-Biotin (Pierce). For endocytosis, cells were warmed to 37°C for different time periods after biotinylation and, subsequently, the disulfide bonds on Sulfo-NHS-SS-biotinylated proteins remaining at the PM were reduced by L-glutathione (GSH; Sigma-Aldrich) at 4 °C. At this point of the protocol, biotinylated proteins reside within the endosomal compartment. Subsequently, cells were lysed, and biotinylated proteins were isolated by streptavidin-agarose beads, eluted into SDS-sample buffer, and separated by SDS-PAGE. The amount of biotinylated

CFTR at 4 °C and without the 37 °C warming was considered 100%. The amount of biotinylated CFTR remaining at the plasma membrane after GSH treatment at 4 °C and without the 37 °C warming was considered background and subtracted from biotinylated CFTR after warming at each time point. CFTR endocytosis was calculated after subtraction of the background and was expressed as the percent of biotinylated CFTR at each time point after warming compared to the amount of biotinylated CFTR present before warming.

For the recycling assay, cells were warmed to 37°C for 5 min after biotinylation, cooled to 4°C and the disulfide bonds on PM proteins reduced by GSH. Following this, cells were either lysed or warmed again to 37°C for different time periods (to allow endocytosed biotinylated CFTR to recycle to the PM). Cells were then cooled again to 4°C and the disulfide bonds on recycled proteins reduced by GSH. The recycling of endocytosed CFTR was calculated as the difference between the amount of biotinylated CFTR after the first and second GSH treatments.

#### *Rap1A activity assay*

The active fraction of Rap with a pull-down assay using the selective interaction of the Rap-binding domain (RBD) of RalGDS with the active, GTP-bound form of Rap, as described (Franke et al., 1997). This domain was expressed tagged with glutathione S-transferase (GST), from bacteria transformed with pGEX-RalGDS-RBDGST, and isolated with glutathione agarose beads (Thermo Scientific). GST-RalGDS-RBD-coupled beads were analysed by SDS-PAGE, confirming that the protein was effectively captured.

For the active Rap1 pull-down, cells were lysed on ice in Rap1A lysis buffer (25mM Tris-HCl, 1% (v/v) NP-40, 5mM MgCl<sub>2</sub>, 150mM NaCl, 0.1mM DTT, 5% (v/v) glycerol, protease

inhibitor cocktail, pH 7.5) for 15min. Lysates were centrifuged and the supernatant was incubated with GST-RalGDS-RBD-coupled beads for 2h at 4°C. Levels of active Rap1A were assessed by WB.

### *Confocal imaging*

Fluorescence imaging was performed 24-48 h after co-transfection of cells with plasmids encoding for GFP-EPAC1 and mCherry-CFTR. Cells were kept at RT in PBS and imaged on an Fluoview FV1000 microscope – an inverted IX81 confocal system (Olympus, Tokyo, Japan) and 60X, NA 1.35 oil immersion UPlanSApo objective (Olympus). Images were acquired using FluoView FV10-ASW software (Olympus) and processed using ImageJ. Intracellular localization of EPAC1 and CFTR in live cells in the absence or presence of 007-AM was monitored and the extent of overlap between the two was quantified using Pearson's correlation coefficient (ImageJ, JACoP plugin)(Zinchuk and Zinchuk, 2008). The overlap between the images of both proteins was analyzed with ImageJ. For fluorescence intensity quantification in a specific region of interest (PM), MetaFluor software (Molecular Devices) was used.

### *Ratio imaging*

Real-time FRET imaging experiments were performed as described (Di Benedetto et al., 2008; Monterisi et al., 2012). cAMP sensor (camps) (DiPilato et al., 2004; Ponsioen et al., 2004), AKAR4 (A-kinase activity reporter 4) (Liu et al., 2011) or Raichu-Rap1 FRET (Mochizuki et al., 2001) sensors were used. FRET imaging experiments were performed 24-48 h after transfection. Cells were maintained at RT or at ~34°C in PBS and imaged on

an inverted microscope (Olympus IX81) using a PlanApoN, 60X, NA 1.42 oil immersion objective, 0.17/FN 26.5 (Olympus). The microscope was equipped with coolSNAP HQ monochrome camera system (Photometrics), hite and 505nm light-emitting diode (LED; Cairn Research) and a beam-splitter optical device (Dual-view simultaneous imaging system, DV2 mag biosystem, Photometrics, ET-04-EM). Images were acquired using MetaFluor or MetaMorph software (Molecular Devices) and processed using ImageJ. FRET changes were measured as changes in the background-subtracted 545/480 nm (AKAR 4 and Raichu-Rap1) or 480nm/545nm (camps) fluorescence emission intensity on excitation at 430 nm and expressed as  $R/R_0$ , where  $R$  is the ratio at time  $t$  and  $R_0$  is the ratio at time = 0 s.

#### *Iodide efflux assay*

The CFTR-mediated iodide efflux assay was performed as described (Mendes et al., 2011). Cells grown in 6-well plates were treated with 1 $\mu$ M 007-AM or 25 $\mu$ M Fsk (or DMSO as control) for 2h, in duplicates. After that, cells were loaded with iodide in the loading buffer for 30 min at 37°C, thoroughly washed with iodide-free efflux buffer and equilibrated for 10 min in the same buffer. Cells were then incubated for 5min either in the presence of iodide-free efflux buffer or in the presence of CFTR stimulators (10 $\mu$ M Fsk and 50 $\mu$ M IBMX, Sigma). Cells were lysed and the iodide concentration in each sample was determined using an iodide-sensitive electrode (Orion 96–53; Thermo Scientific, Rockford, IL, U.S.A) with a pH/mV meter and normalized to the amount of protein. In this assay, increased channel activity corresponds to more iodide released from the cells and thus decreased iodide concentration remaining within the cells.

### *Statistical Analysis*

Data are presented as a mean standard error of the mean (SEM), as indicated in figure legends. Data were analyzed using student's t-test, with  $p < 0.05$  accepted as the level of statistical significance. The number of biological replicates is indicated in figure legends. Error bars reflect independent experiments.

## **Acknowledgements**

We are grateful to the following individuals for their kind gifts of plasmids: Dr.Kees Jalink (NKI, Netherlands) for the EPAC1 constructs, Prof.Michiyuki Matsuda (Kyoto Univ, Japan) for the Raichu sensors, Dr.Paulo Matos (INSA, Portugal) and Prof.Valeria Casavola (Univ Bari, Italy) for the NHERF1 constructs, and Prof.David Altschuler (Univ Pittsburgh School of Medicine, USA) for the pGEX-RalGDS-RBDGST plasmid. We thank to Konstantinos Lefkimmiatis for the PKI-mCherry plasmid and for helpful comments and Inna Uliyakina, José Múrias, Stefania Monterisi and Andreas Koschinski for assistance.

## **Funding**

Work supported by Fundação para a Ciência e Tecnologia (grant UID/MULTI/04046/2013 to BioISI and grant EXPL/BIM-MEC/1451/2013 to C.M.F.), European Respiratory Society (Romain Pauwels Research Award to C.M.F.) and British Heart Foundation (grants PG/15/5/31110 and RG/12/3/29423 to M.Z.).

## **Author contribution**

M.J.L. designed and performed the experiments, analyzed data and wrote the paper; M.D.A. provided advice and comments on the paper; M.Z. designed the experiments, provided advice, support, and comments on the paper. C.M.F. guided the project, designed the experiments, analyzed data and wrote the paper.

## Figure legends

**Figure 1: CFTR surface expression and endocytosis under EPAC1 activation.** (A) CFBE-wt cells treated with increasing concentrations of Fsk (alone or together with 100 $\mu$ M IBMX) for 2h were subjected to cell surface biotinylation (non-biotinylated samples - negative control). After streptavidin pull-down, CFTR was detected by WB. Ezrin was not detected in the biotinylated fraction. CFTR, calnexin, ezrin and tubulin are detected in the whole cell lysate (WCL) as a control. (B) Quantification of CFTR at the PM, normalized to the amount of total CFTR and shown as fold change relatively to 0.01 $\mu$ M Fsk. Data represent mean  $\pm$  SEM (n=5). (C) Quantification of CFTR at the PM for the 50 $\mu$ M Fsk+100 $\mu$ M IBMX treatment and shown as fold change relatively to 50 $\mu$ M Fsk treatment. Data represent mean  $\pm$  SEM (n=4). (D) CFBE-wt cells treated with 1 $\mu$ M 6-Bnz-cAMP-AM or 007-AM for 2h (or DMSO as control) were biotinylated as in A. (E) Quantification of CFTR at the PM, normalized to total CFTR and shown as fold change relatively to DMSO. Data represent mean  $\pm$  SEM (n=6-9). (F) CFBE-wt cells transfected with PKI (or control vector – no PKI) were biotinylated as in A. (G) Quantification of CFTR at the PM normalized to total CFTR and shown as fold change relatively to no PKI control. Data represent mean  $\pm$  SEM. (n=4). (H) CFBE-wt cells treated with 1 $\mu$ M 007-AM for 2h (or DMSO as control) or transfected with siRNA against EPAC1 (non-targeting siRNA - control) were biotinylated as in A. (I) Quantification of CFTR at the PM normalized to total CFTR and shown as fold change relatively to siRNA control. Data represent mean  $\pm$  SEM. (n=3). (J) Quantification of total EPAC1 normalized to calnexin, shown as fold change relatively to siRNA control. Data represent mean  $\pm$  SEM (n=3). (K) Iodide efflux of CFBE-wt cells treated with 1 $\mu$ M 007-AM, 1 $\mu$ M 6-Bnz-cAMP-AM, 1 $\mu$ M 007-AM combined with 1 $\mu$ M 6-Bnz-cAMP-AM or 25 $\mu$ M Fsk (or DMSO as control) for 2h. Fold change of iodide that

remained in the cells relative to control condition. Data represent mean  $\pm$  SEM. (n=5). ‘\*’ indicates significance for  $p < 0.05$ .

**Figure 2: CFTR endocytosis and recycling under EPAC1 activation.** (A) CFBE-wt cells treated with 1 $\mu$ M 007-AM for 2h (or DMSO as control) were biotinylated, followed by incubation at 37°C (during 2.5, 5 or 10 minutes). After that, cells were treated with a GSH solution and, after cell lysis and streptavidin pull-down, CFTR was detected by WB (samples not treated with GSH – positive control; samples not incubated at 37°C – negative control). (B) Quantification of internalized CFTR. The negative (-) control was subtracted from the amount of endocytosed CFTR and values were normalized to the positive (+) control. Data represent mean  $\pm$  SEM (n=3-7). (C) CFBE-wt cells treated with 1 $\mu$ M 007-AM or 25 $\mu$ M Fsk for 2h (or DMSO as control), in combination or not with 80 $\mu$ M Dynasore, were biotinylated and CFTR was detected by WB as in A. (D) Quantification of CFTR at the PM, normalized to the amount of total CFTR and shown as fold change relatively to DMSO. Data represent mean  $\pm$  SEM (n=3). (E) To assess recycling of CFTR, endocytosis was induced for 5 min, as in A, in CFBE-wt cells treated with 1 $\mu$ M 007-AM for 2h (or DMSO as control), followed by incubation at 37°C (during 2.5, 5 or 10 minutes) after GSH treatment. After that, cells were treated for a second time with a GSH solution and, after cell lysis and streptavidin pull-down, CFTR was detected by WB (samples not treated with GSH – positive control; samples not incubated at 37°C – negative control). (F) Quantification of the percentage of recycled CFTR relative to the amount of endocytosed CFTR. CFTR recycling was calculated as the difference between the amount of biotinylated CFTR after the first and second GSH treatments. Data represent mean  $\pm$  SEM (n=3-4). ‘\*’ indicates significance for  $p < 0.05$ .

**Figure 3: EPAC1 co-localization with CFTR after treatment with 007-AM in CFBE cells.** (A) Confocal live cell imaging analysis of GFP-EPAC1 localization in CFBE cells. Images show EPAC1 staining before (upper panels) and 6 min after addition of 1 $\mu$ M 007-AM (lower panels). Scale bars, 10  $\mu$ m. (B) Percentage of cells showing translocation of EPAC1 to the PM upon 007-AM stimulation (Consonni et al., 2012) (n=11-40 cells, 5-21 experiments). (C) Fluorescence pixel intensity of GFP-EPAC1 at the PM versus cytosol during stimulation with 1 $\mu$ M 007-AM relative to pre-stimulus levels in CFBE parental, CFBE-wt and CFBE-F508del cells. Images were acquired every 3 min with 007-AM added after the acquisition at minute 3 (*Figure S3C*). RFU, Relative Fluorescence Units. Confocal live-cell imaging analysis of (D) mCherry-wt-CFTR or (E) mCherry-F508del-CFTR and GFP-EPAC1 in transiently transfected CFBE cells. Images show EPAC1 staining before (upper panels) and 6 min after addition of 1 $\mu$ M 007-AM (lower panels). Scale bars, 10  $\mu$ m. (F) Pearson's Coefficient fold increase analysis from D and E. Any value above the dotted line is considered significant for co-localization (Zinchuk and Zinchuk, 2008). Data represent mean  $\pm$  SEM (n=9/18 cells, 7/5 experiments) (wt-/F508del-CFTR). ‘\*\*’ indicates significance for  $p < 0.05$ .

**Figure 4: Interaction of CFTR and EPAC1.** (A) Detection of GFP-EPAC1 after mCherry-wt-CFTR immunoprecipitation in CFBE cells transfected with GFP-EPAC1 and mCherry-wt-CFTR. Pull-down with beads only (without conjugated antibody) was used as a negative control. (B) Detection of CFTR after immunoprecipitation of constitutive EPAC1 from CFBE-wt cells. (C) Quantification of CFTR-EPAC1 interaction fold increase after treatment with 007-AM in CFBE-wt cells. Amount of precipitated EPAC1 was normalized to the amount of immunoprecipitated CFTR and shown as fold change relatively to DMSO

treated cells. Data represent mean  $\pm$  SEM (n=6). **(D)** Detection of CFTR after EPAC1 immunoprecipitation and detection of EPAC1 after CFTR immunoprecipitation from A549-wt/F508del cells treated with 1 $\mu$ M 007-AM for 2h (or DMSO as control). **(E and F)** Quantification of CFTR-EPAC1 interaction fold increase after treatment with 007-AM in A549-wt/F508del cells. Amount of precipitated CFTR (E) or EPAC1 (F) was normalized to the amount of immunoprecipitated EPAC1 or CFTR, respectively, and shown as fold change relatively to DMSO treated cells. Data represent mean  $\pm$  SEM. n=3-5. “\*” indicates significance for  $p < 0.05$ .

**Figure 5: Interaction of CFTR and EPAC1 under down-regulation of ezrin or NHERF1.** **(A)** Detection of EPAC1 after immunoprecipitation of CFTR from CFBE-wt cells transiently transfected with ezrin or NHERF1siRNA (non-targeting siRNA used as control). **(B)** Amount of precipitated EPAC1 was normalized to immunoprecipitated CFTR and shown as fold change relatively to control. **(C)** Quantification of total ezrin or NHERF1 after siRNA transfection (siRNA ezrin and NHERF1, respectively), normalized to  $\alpha$ -tubulin/calnexin and shown as fold change relatively to control. Data represent mean  $\pm$  SEM (n=4). **(D)** Detection of EPAC1 after immunoprecipitation of CFTR from Calu3 cells stably transduced with shRNA against ezrin or NHERF1. Empty lentiviral vector was used as shRNA control. **(E)** Amount of precipitated EPAC1 was normalized to immunoprecipitated CFTR and shown as fold change relatively to control. **(F)** Quantification of ezrin or NHERF1 after shRNA transduction (shEzrin or shNHERF1, respectively) normalized to  $\alpha$ -tubulin/calnexin, respectively, and relative to the amount of these proteins when shControl was used. Data represent mean  $\pm$  SEM (n=3). **(G)** CFTR expression at the PM in CFBE-wt cells under ezrin or NHERF1 down-regulation. Cells were biotinylated as in Fig.1A biotinylation and CFTR levels were assessed by WB(non-

targeting siRNA used as control). **(H)** Quantification of CFTR at the PM for each siRNA, normalized to the amount of total CFTR and shown as fold change relatively to DMSO treated cells. Data represent mean  $\pm$  SEM.  $n=3$ . “\*” indicates significance for  $p<0.05$ .

**Figure 6: Interaction of EPAC1 and NHERF1.** **(A)** Detection of NHERF1 after immunoprecipitation of EPAC1 from CFBE-wt cells. Pull-down with beads only was used as negative control. **(B)** Detection of GFP-EPAC1 (GFP) after immunoprecipitation of Myc-NHERF1 (Myc) and detection of Myc-NHERF1 (Myc) after immunoprecipitation of GFP-EPAC1 (GFP) from transiently transfected HEK293T cells. **(C)** Detection of Myc-NHERF1 after immunoprecipitation of GFP-EPAC1 in transiently transfected HEK293T cells treated with 1 $\mu$ M 007-AM for 2h (or DMSO as control). **(D)** Quantification of EPAC1-NHERF1 interaction fold increase after treatment with 007-AM in HEK293T cells transiently transfected with GFP-EPAC1 and Myc-NHERF1. Amount of precipitated Myc-NHERF1 was normalized to immunoprecipitated GFP-EPAC1 and shown as fold change relatively to DMSO incubated cells. Data represent mean  $\pm$  SEM ( $n=3$ ). “\*” indicates significance for  $p<0.05$ .

**Figure 7: EPAC1 activation increases F508del-CFTR rescue.** **(A)** CFBE-F508del cells were treated with 1 $\mu$ M 007-AM, 3 $\mu$ M VX-809 or both (DMSO used as negative control) for 24 or 48h. CFTR steady state levels were assessed by WB. **(B)** CFTR processing (amount of band C normalized to total amount CFTR – band C + band B) shown as a fold increase relatively to VX-809-treated cells. Data represent mean  $\pm$  SEM ( $n=8-10$ ). **(C)** Iodide efflux of CFBE-F508del cells treated with 3 $\mu$ M VX-809 and 1 $\mu$ M 007-AM (or DMSO as control) for 2h. Fold change of the amount of iodide that remained in the cells relative to VX-809

only cells. Data represent mean  $\pm$  SEM. (n=11). ‘\*’ indicates significance for  $p < 0.05$ . (D) Binding to NHERF1 anchors CFTR (via ezrin) to the actin cytoskeleton. In cells with low levels of cAMP near the PM, EPAC1 is inactive and its interaction with CFTR is not promoted. In cells with high levels of cAMP near the PM, both PKA and EPAC1 are active, promoting the opening of the channel and stabilizing CFTR at the PM, respectively. PDZ - PSD95, Dlg1, ZO-1 binding motif.

## References

- Almaca, J., Dahimene, S., Appel, N., Conrad, C., Kunzelmann, K., Pepperkok, R. and Amaral, M. D.** (2011). Functional genomics assays to study CFTR traffic and ENaC function. *Meth Mol Biol* **742**, 249-64.
- Amaral, M. D. and Farinha, C. M.** (2013). Rescuing mutant CFTR: a multi-task approach to a better outcome in treating cystic fibrosis. *Curr Pharm Des* **19**, 3497-508.
- Bebok, Z., Collawn, J. F., Wakefield, J., Parker, W., Li, Y., Varga, K., Sorscher, E. J. and Clancy, J. P.** (2005). Failure of cAMP agonists to activate rescued deltaF508 CFTR in CFBE41o- airway epithelial monolayers. *J Physiol* **569**, 601-15.
- Boucher, R. C.** (2004). New concepts of the pathogenesis of cystic fibrosis lung disease. *Eur Respir J* **23**, 146-58.
- Castellani, S., Guerra, L., Favia, M., Di Gioia, S., Casavola, V. and Conese, M.** (2012). NHERF1 and CFTR restore tight junction organisation and function in cystic fibrosis airway epithelial cells: role of ezrin and the RhoA/ROCK pathway. *Lab Invest* **92**, 1527-40.
- Chang, S. Y., Di, A., Naren, A. P., Palfrey, H. C., Kirk, K. L. and Nelson, D. J.** (2002). Mechanisms of CFTR regulation by syntaxin 1A and PKA. *J Cell Sci* **115**, 783-91.
- Christensen, A. E., Selheim, F., de Rooij, J., Dremier, S., Schwede, F., Dao, K. K., Martinez, A., Maenhaut, C., Bos, J. L., Genieser, H. G. et al.** (2003). cAMP analog mapping of Epac1 and cAMP kinase. Discriminating analogs demonstrate that Epac and cAMP kinase act synergistically to promote PC-12 cell neurite extension. *J Biol Chem* **278**, 35394-402.
- Cihil, K. M., Ellinger, P., Fellows, A., Stolz, D. B., Madden, D. R. and Swiatecka-Urban, A.** (2012). Disabled-2 protein facilitates assembly polypeptide-2-independent recruitment of cystic fibrosis transmembrane conductance regulator to endocytic vesicles in polarized human airway epithelial cells. *J Biol Chem* **287**, 15087-99.
- Clancy, J. P., Rowe, S. M., Accurso, F. J., Aitken, M. L., Amin, R. S., Ashlock, M. A., Ballmann, M., Boyle, M. P., Bronsveld, I., Campbell, P. W. et al.** (2012). Results of a phase IIa study of VX-809, an investigational CFTR corrector compound, in subjects with cystic fibrosis homozygous for the F508del-CFTR mutation. *Thorax* **67**, 12-18.
- Conrotto, P., Yakymovych, I., Yakymovych, M. and Souchelnytskyi, S.** (2007). Interactome of transforming growth factor-beta type I receptor (TbetaRI): inhibition of TGFbeta signaling by Epac1. *J Proteome Res* **6**, 287-97.
- Consonni, S. V., Gloerich, M., Spanjaard, E. and Bos, J. L.** (2012). cAMP regulates DEP domain-mediated binding of the guanine nucleotide exchange factor Epac1 to phosphatidic acid at the plasma membrane. *Proc Natl Acad Sci U S A* **109**, 3814-9.
- de Rooij, J., Rehmann, H., van Triest, M., Cool, R. H., Wittinghofer, A. and Bos, J. L.** (2000). Mechanism of regulation of the Epac family of cAMP-dependent RapGEFs. *J Biol Chem* **275**, 20829-36.
- DiPilato, L. M., Cheng, X. and Zhang, J.** (2004). Fluorescent indicators of cAMP and Epac activation reveal differential dynamics of cAMP signaling within discrete subcellular compartments. *Proc Natl Acad Sci U S A* **101**, 16513-8.
- Farinha, C. M., King-Underwood, J., Sousa, M., Correia, A. R., Henriques, B. J., Roxo-Rosa, M., Da Paula, A. C., Williams, J., Hirst, S., Gomes, C. M. et al.** (2013a). Revertants, low temperature, and correctors reveal the mechanism of F508del-CFTR rescue by VX-809 and suggest multiple agents for full correction. *Chem Biol* **20**, 943-55.
- Farinha, C. M., Matos, P. and Amaral, M. D.** (2013b). Control of CFTR membrane trafficking: not just from the ER to the Golgi. *FEBS J.* **280**, 4396-406.

- Farinha, C. M., Nogueira, P., Mendes, F., Penque, D. and Amaral, M. D.** (2002). The human DnaJ homologue (Hdj)-1/heat-shock protein (Hsp) 40 co-chaperone is required for the in vivo stabilization of the cystic fibrosis transmembrane conductance regulator by Hsp70. *Biochem J* **366**, 797-806.
- Favia, M., Guerra, L., Fanelli, T., Cardone, R. A., Monterisi, S., Di Sole, F., Castellani, S., Chen, M., Seidler, U., Reshkin, S. J. et al.** (2010). Na<sup>+</sup>/H<sup>+</sup> exchanger regulatory factor 1 overexpression-dependent increase of cytoskeleton organization is fundamental in the rescue of F508del cystic fibrosis transmembrane conductance regulator in human airway CFBE41o- cells. *Mol Biol Cell* **21**, 73-86.
- Franke, B., Akkerman, J. W. and Bos, J. L.** (1997). Rapid Ca<sup>2+</sup>-mediated activation of Rap1 in human platelets. *EMBO J* **16**, 252-9.
- Gloerich, M. and Bos, J. L.** (2010). Epac: defining a new mechanism for cAMP action. *Annu Rev Pharmacol Toxicol* **50**, 355-75.
- Gloerich, M., Ponsioen, B., Vliem, M. J., Zhang, Z., Zhao, J., Kooistra, M. R., Price, L. S., Ritsma, L., Zwartkuis, F. J., Rehmann, H. et al.** (2010). Spatial regulation of cyclic AMP-Epac1 signaling in cell adhesion by ERM proteins. *Mol Cell Biol* **30**, 5421-31.
- Gruenert, D. C., Finkbeiner, W. E. and Widdicombe, J. H.** (1995). Culture and transformation of human airway epithelial cells. *Am J Physiol* **268**, L347-L360.
- Haggie, P. M., Kim, J. K., Lukacs, G. L. and Verkman, A. S.** (2006). Tracking of quantum dot-labeled CFTR shows near immobilization by C-terminal PDZ interactions. *Mol Biol Cell* **17**, 4937-45.
- Hoque, K. M., Woodward, O. M., van Rossum, D. B., Zachos, N. C., Chen, L., Leung, G. P., Guggino, W. B., Guggino, S. E. and Tse, C. M.** (2010). Epac1 mediates protein kinase A-independent mechanism of forskolin-activated intestinal chloride secretion. *J Gen Physiol* **135**, 43-58.
- Ivonnet, P., Salathe, M. and Conner, G. E.** (2015). Hydrogen peroxide stimulation of CFTR reveals an Epac-mediated, soluble AC-dependent cAMP amplification pathway common to GPCR signalling. *Br J Pharmacol* **172**, 173-84.
- Kooistra, M. R., Corada, M., Dejana, E. and Bos, J. L.** (2005). Epac1 regulates integrity of endothelial cell junctions through VE-cadherin. *FEBS Lett* **579**, 4966-72.
- Lefkimmiatis, K., Leronni, D. and Hofer, A. M.** (2013). The inner and outer compartments of mitochondria are sites of distinct cAMP/PKA signaling dynamics. *J Cell Biol* **202**, 453-62.
- Li, J., Dai, Z., Jana, D., Callaway, D. J. and Bu, Z.** (2005). Ezrin controls the macromolecular complexes formed between an adapter protein Na<sup>+</sup>/H<sup>+</sup> exchanger regulatory factor and the cystic fibrosis transmembrane conductance regulator. *J Biol Chem* **280**, 37634-43.
- Liu, S., Zhang, J. and Xiang, Y. K.** (2011). FRET-based direct detection of dynamic protein kinase A activity on the sarcoplasmic reticulum in cardiomyocytes. *Biochem Biophys Res Commun* **404**, 581-6.
- Loureiro, C. A., Matos, A. M., Dias-Alves, A., Pereira, J. F., Uliyakina, I., Barros, P., Amaral, M. D. and Matos, P.** (2015). A molecular switch in the scaffold NHERF1 enables misfolded CFTR to evade the peripheral quality control checkpoint. *Sci Signal* **8**, ra48.
- Macia, E., Ehrlich, M., Massol, R., Boucrot, E., Brunner, C. and Kirchhausen, T.** (2006). Dynasore, a cell-permeable inhibitor of dynamin. *Developmental cell* **10**, 839-50.
- Mendes, A. I., Matos, P., Moniz, S., Luz, S., Amaral, M. D., Farinha, C. M. and Jordan, P.** (2011). Antagonistic Regulation of CFTR Cell Surface Expression by Protein Kinases WNK4 and Spleen Tyrosine Kinase. *Mol Cell Biol* **19**, 4076-4086.

**Mochizuki, N., Yamashita, S., Kurokawa, K., Ohba, Y., Nagai, T., Miyawaki, A. and Matsuda, M.** (2001). Spatio-temporal images of growth-factor-induced activation of Ras and Rap1. *Nature* **411**, 1065-8.

**Monterisi, S., Casavola, V. and Zaccolo, M.** (2013). Local modulation of cystic fibrosis conductance regulator: cytoskeleton and compartmentalized cAMP signalling. *Br J Pharmacol* **169**, 1-9.

**Monterisi, S., Favia, M., Guerra, L., Cardone, R. A., Marzulli, D., Reshkin, S. J., Casavola, V. and Zaccolo, M.** (2012). CFTR regulation in human airway epithelial cells requires integrity of the actin cytoskeleton and compartmentalized cAMP and PKA activity. *J Cell Sci* **125**, 1106-17.

**Morales, F. C., Takahashi, Y., Momin, S., Adams, H., Chen, X. and Georgescu, M. M.** (2007). NHERF1/EBP50 head-to-tail intramolecular interaction masks association with PDZ domain ligands. *Mol Cell Biol* **27**, 2527-37.

**Nakamura, T., Kurokawa, K., Kiyokawa, E. and Matsuda, M.** (2006). Analysis of the spatiotemporal activation of rho GTPases using Raichu probes. *Methods Enzymol* **406**, 315-32.

**Ponsioen, B., Gloerich, M., Ritsma, L., Rehmann, H., Bos, J. L. and Jalink, K.** (2009). Direct spatial control of Epac1 by cyclic AMP. *Mol Cell Biol* **29**, 2521-31.

**Ponsioen, B., Zhao, J., Riedl, J., Zwartkruis, F., van der Krogt, G., Zaccolo, M., Moolenaar, W. H., Bos, J. L. and Jalink, K.** (2004). Detecting cAMP-induced Epac activation by fluorescence resonance energy transfer: Epac as a novel cAMP indicator. *EMBO Rep* **5**, 1176-80.

**Reczek, D., Berryman, M. and Bretscher, A.** (1997). Identification of EBP50: A PDZ-containing phosphoprotein that associates with members of the ezrin-radixin-moesin family. *J Cell Biol* **139**, 169-179.

**Riordan, J. R.** (2008). CFTR function and prospects for therapy. *Annu Rev Biochem* **77**, 701-26.

**Roscioni, S. S., Kistemaker, L. E., Menzen, M. H., Elzinga, C. R., Gosens, R., Halayko, A. J., Meurs, H. and Schmidt, M.** (2009). PKA and Epac cooperate to augment bradykinin-induced interleukin-8 release from human airway smooth muscle cells. *Respiratory research* **10**, 88.

**Schmidt, M., Dekker, F. J. and Maarsingh, H.** (2013). Exchange protein directly activated by cAMP (epac): a multidomain cAMP mediator in the regulation of diverse biological functions. *Pharmacol Rev* **65**, 670-709.

**Schwede, F., Bertinetti, D., Langerijs, C. N., Hadders, M. A., Wienk, H., Ellenbroek, J. H., de Koning, E. J., Bos, J. L., Herberg, F. W., Genieser, H. G. et al.** (2015). Structure-guided design of selective Epac1 and Epac2 agonists. *PLoS Biol* **13**, e1002038.

**Sheppard, D. N. and Welsh, M. J.** (1999). Structure and function of the CFTR chloride channel. *Physiol Rev* **79**, S23-S45.

**Sun, F., Hug, M. J., Bradbury, N. A. and Frizzell, R. A.** (2000a). Protein kinase A associates with cystic fibrosis transmembrane conductance regulator via an interaction with ezrin. *J Biol Chem* **275**, 14360-6.

**Sun, F., Hug, M. J., Lewarchik, C. M., Yun, C. H., Bradbury, N. A. and Frizzell, R. A.** (2000b). E3KARP mediates the association of ezrin and protein kinase A with the cystic fibrosis transmembrane conductance regulator in airway cells. *J Biol Chem* **275**, 29539-46.

**Swiatecka-Urban, A., Duhaime, M., Coutermarsh, B., Karlson, K. H., Collawn, J., Milewski, M., Cutting, G. R., Guggino, W. B., Langford, G. and Stanton, B. A.** (2002). PDZ domain interaction controls the endocytic recycling of the cystic fibrosis transmembrane conductance regulator. *J Biol Chem* **277**, 40099-105.

**Tkachenko, E., Sabouri-Ghomi, M., Pertz, O., Kim, C., Gutierrez, E., Machacek, M., Groisman, A., Danuser, G. and Ginsberg, M. H.** (2011). Protein kinase A governs a RhoA-RhoGDI protrusion-retraction pacemaker in migrating cells. *Nature Cell Biol* **13**, 660-7.

**Ulucan, C., Wang, X., Baljinnyam, E., Bai, Y., Okumura, S., Sato, M., Minamisawa, S., Hirotani, S. and Ishikawa, Y.** (2007). Developmental changes in gene expression of Epac and its upregulation in myocardial hypertrophy. *Am J Physiol Heart Circ Physiol* **293**, H1662-72.

**Van Goor, F., Hadida, S., Grootenhuys, P. D., Burton, B., Stack, J. H., Straley, K. S., Decker, C. J., Miller, M., McCartney, J., Olson, E. R. et al.** (2011). Correction of the F508del-CFTR protein processing defect in vitro by the investigational drug VX-809. *Proc Natl Acad Sci U S A* **108**, 18843-18848.

**Voltz, J. W., Weinman, E. J. and Shenolikar, S.** (2001). Expanding the role of NHERF, a PDZ-domain containing protein adapter, to growth regulation. *Oncogene* **20**, 6309-14.

**Wainwright, C. E., Elborn, J. S., Ramsey, B. W., Marigowda, G., Huang, X., Cipolli, M., Colombo, C., Davies, J. C., De Boeck, K., Flume, P. A. et al.** (2015). Lumacaftor-Ivacaftor in Patients with Cystic Fibrosis Homozygous for Phe508del CFTR. *N Engl J Med* **373**, 220-31.

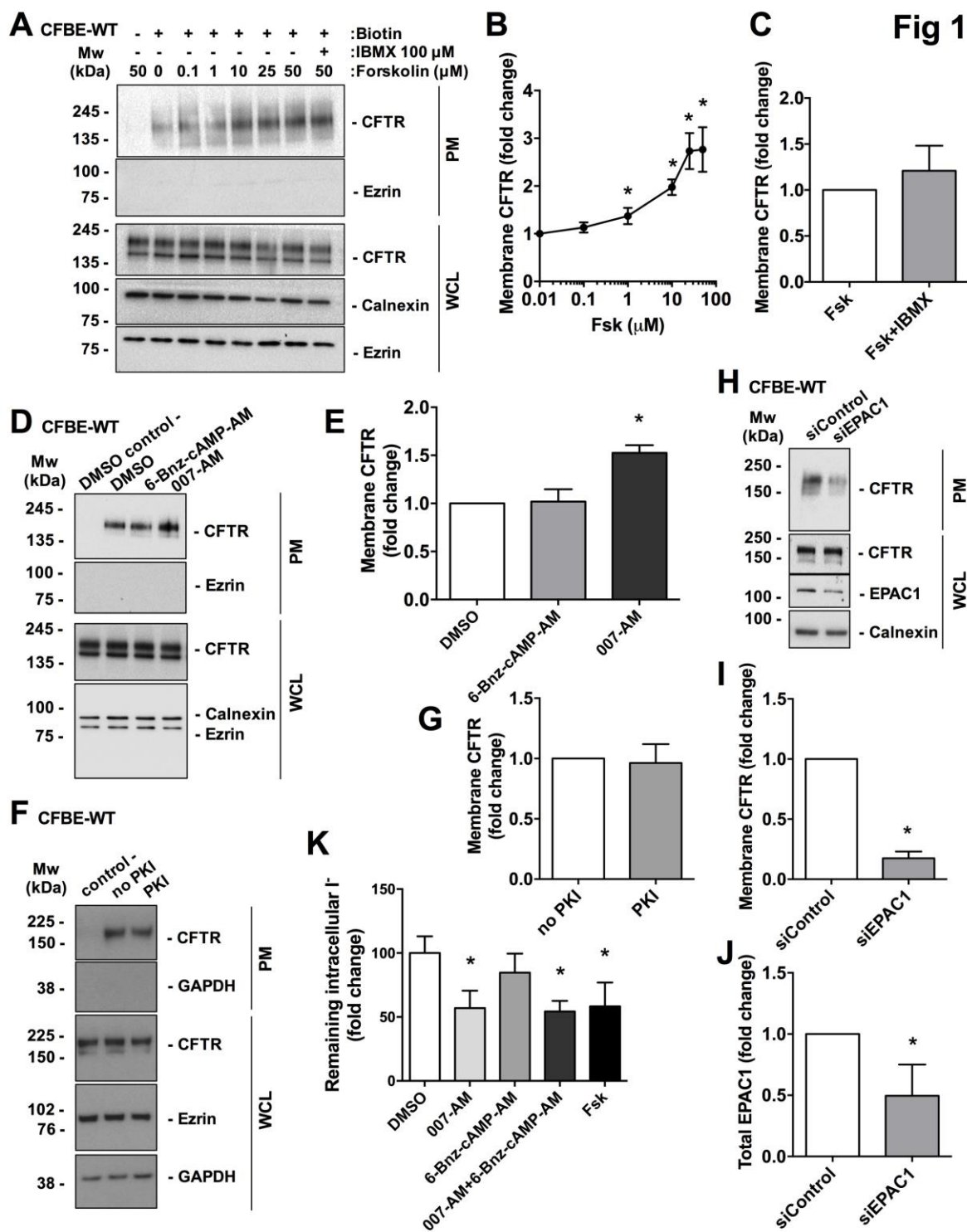
**Wang, S., Raab, R. W., Schatz, P. J., Guggino, W. B. and Li, M.** (1998). Peptide binding consensus of the NHE-RF-PDZ1 domain matches the C- terminal sequence of cystic fibrosis transmembrane conductance regulator (CFTR). *FEBS Lett.* **427**, 103-108.

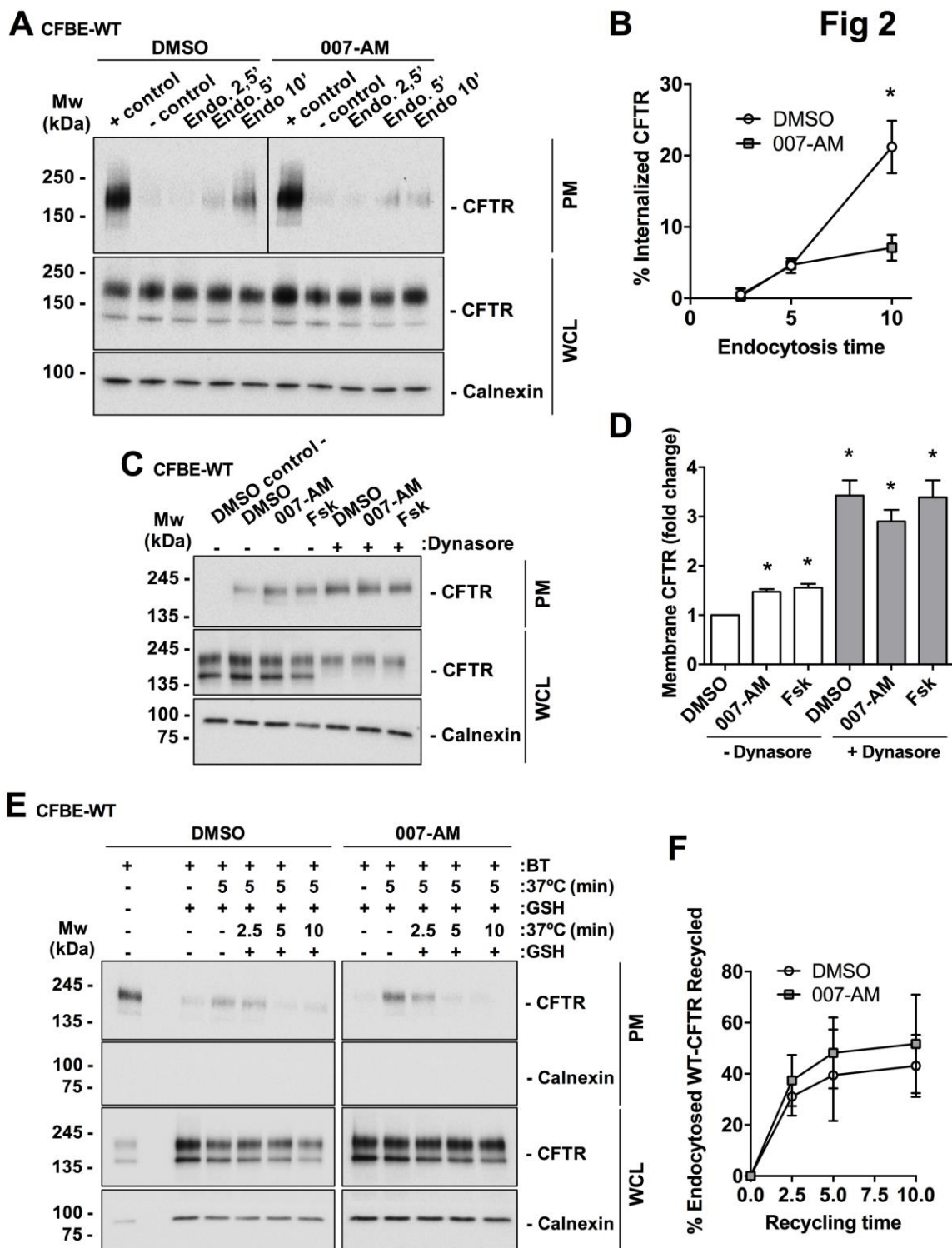
**Young, A., Gentzsch, M., Abban, C. Y., Jia, Y., Meneses, P. I., Bridges, R. J. and Bradbury, N. A.** (2009). Dynasore inhibits removal of wild-type and DeltaF508 cystic fibrosis transmembrane conductance regulator (CFTR) from the plasma membrane. *Biochem J* **421**, 377-85.

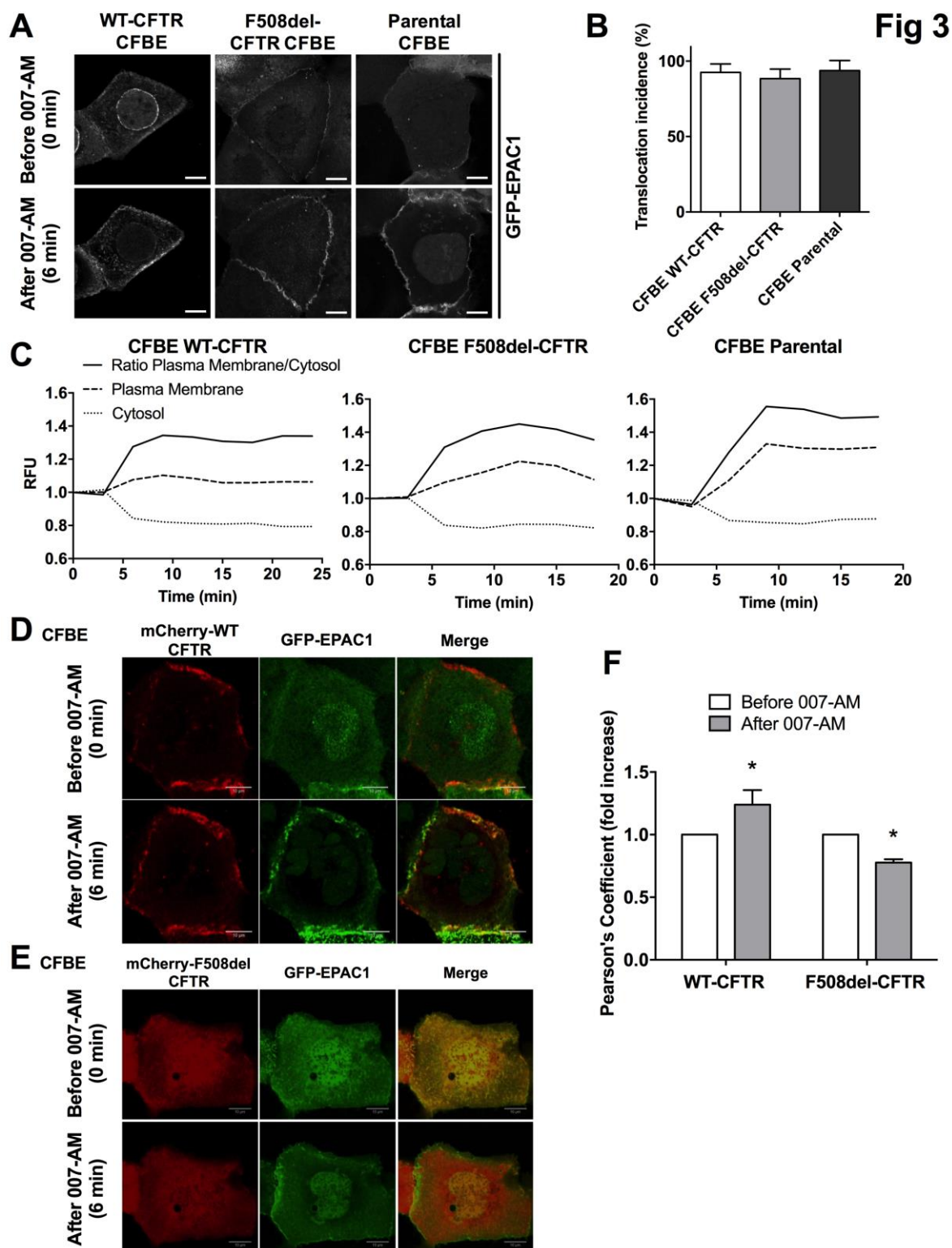
**Zinchuk, V. and Zinchuk, O.** (2008). Quantitative colocalization analysis of confocal fluorescence microscopy images. *Current protocols in cell biology* **Chapter 4**, Unit 4 19.

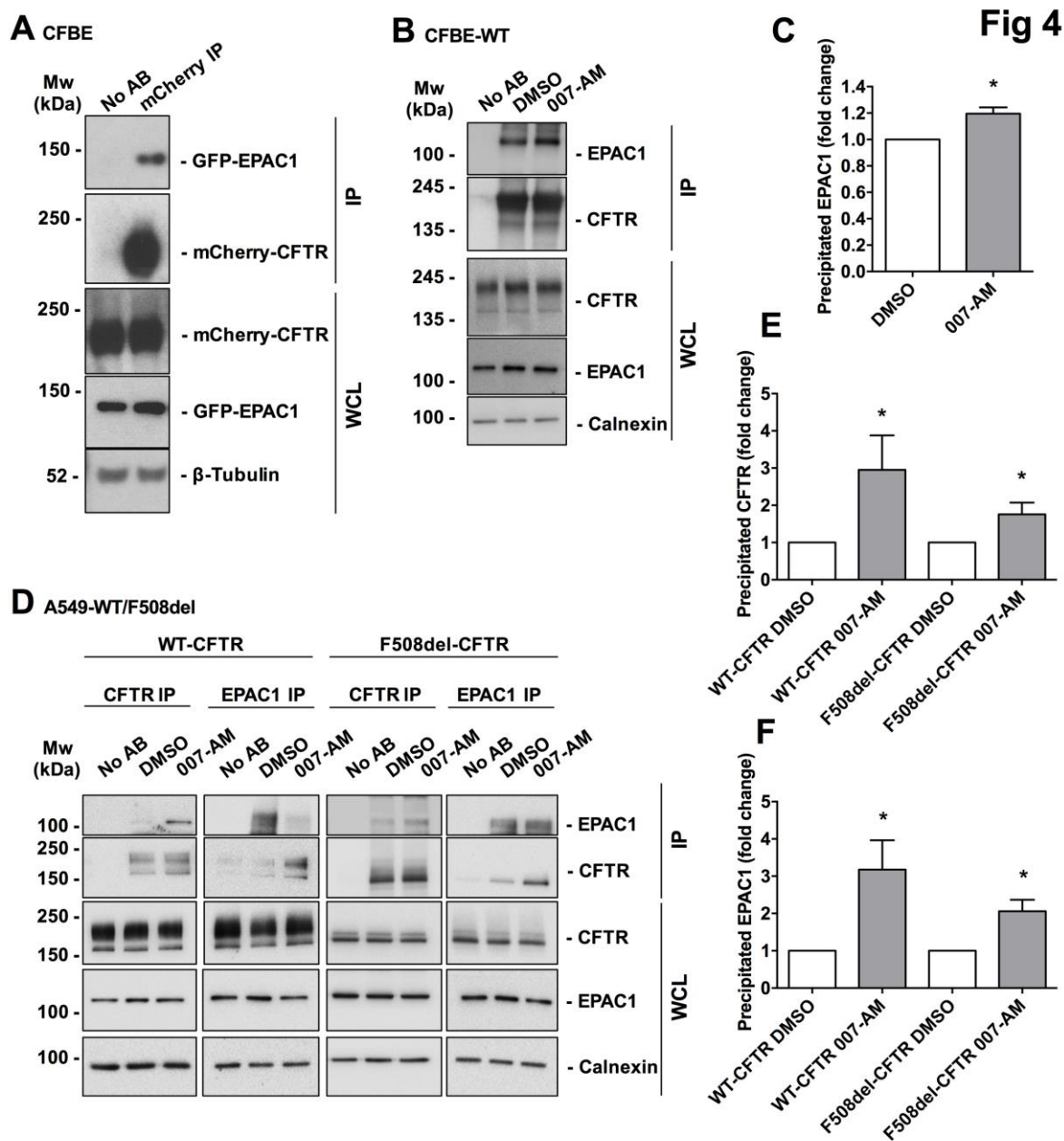
**Abbreviations List**

007-AM, 8-(4-Chlorophenylthio)-2'-O-methyladenosine-3',5'-cyclic monophosphate acetoxymethyl ester (8-pCPT-2'-O-Me-cAMP-AM); ABC, ATP-binding cassette; CF, cystic fibrosis; CFBE41o- / CFBE, cystic fibrosis bronchial epithelial (cell line); CFBE-wt, CFBE cells expressing wt-CFTR; CFTR, cystic fibrosis transmembrane conductance regulator; EPAC; exchange protein directly activated by cAMP; ERM, ezrin/radixin/moesin; Fsk, forskolin; GEF, guanine nucleotide exchange factor; IBMX, 3-isobutyl-1-methylxanthine; NBD nucleotide binding domain; NHERF, Na<sup>+</sup>/H<sup>+</sup>-exchanger regulatory factor; PKA, protein kinase A; PKI, protein kinase A inhibitor; PM, plasma membrane; RD, regulatory domain; TGN, trans-Golgi network; TMD, transmembrane domain; WCL, Whole cell lysate.









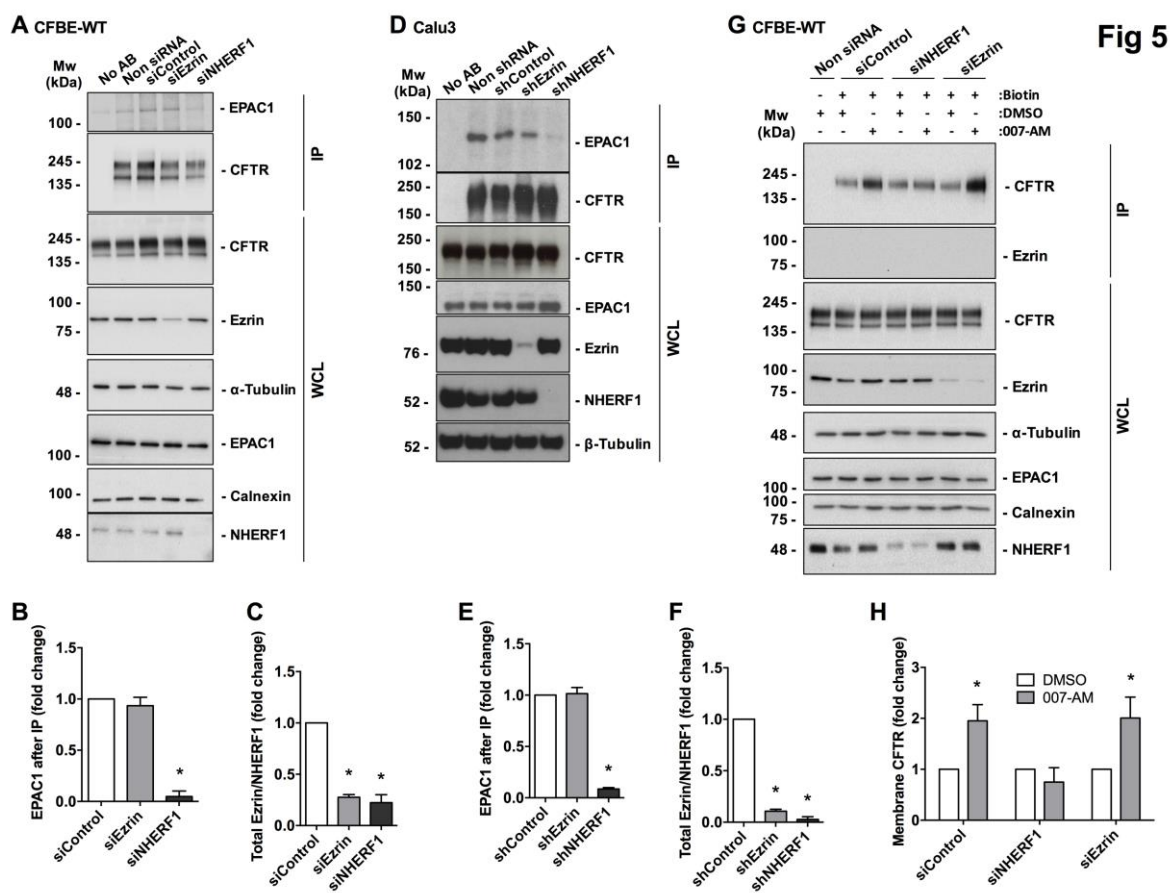
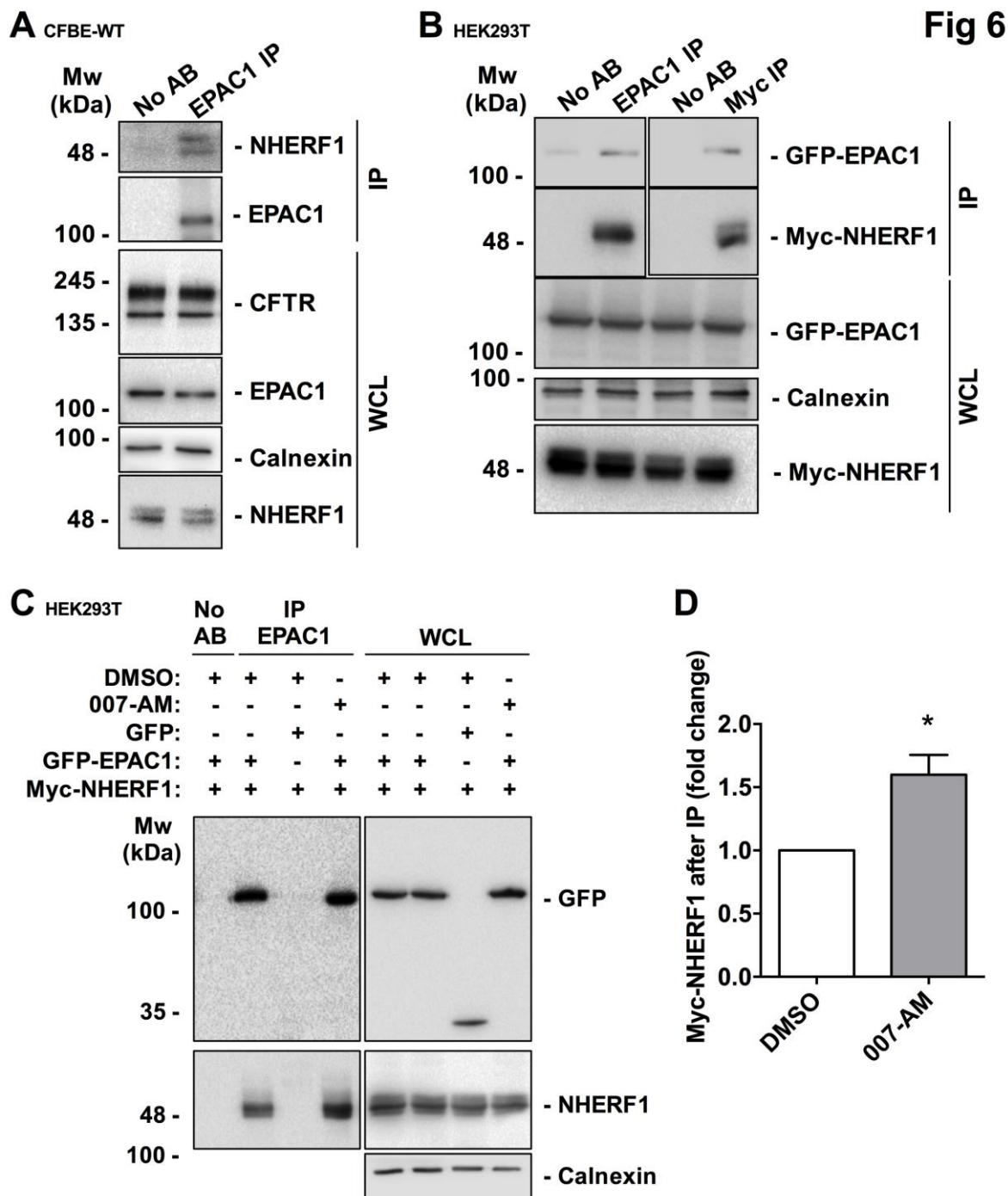
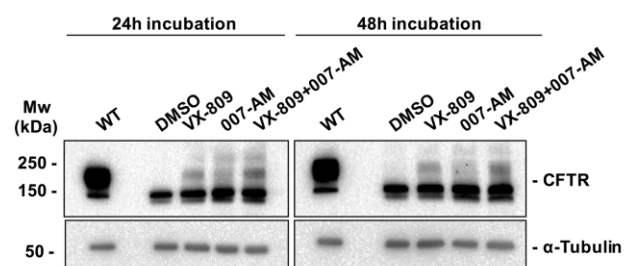
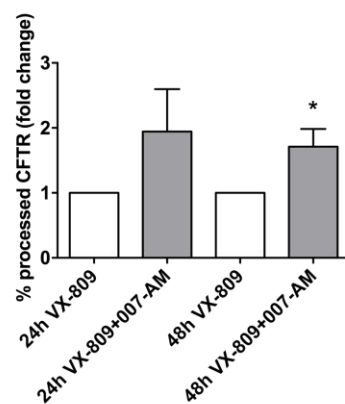
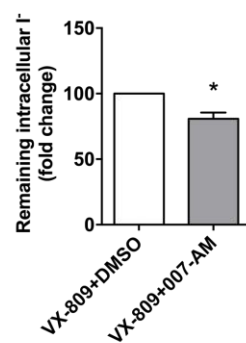
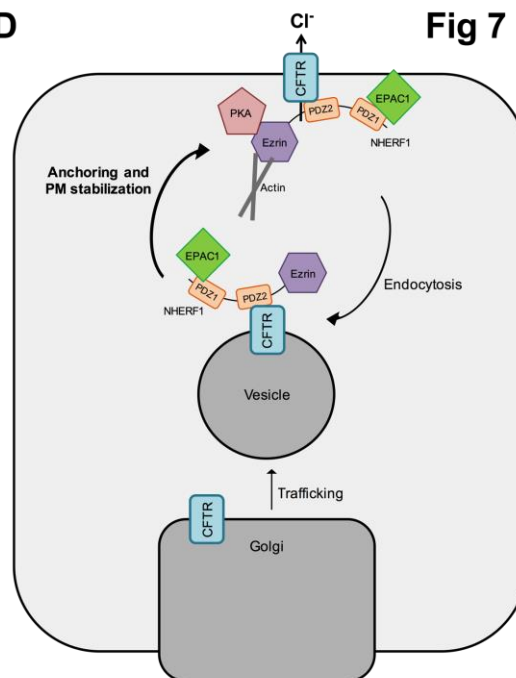


Fig 5



**A** CFBE-F508del**B****C****D****Fig 7**

**Supplementary Information**

**EPAC1 activation by cAMP stabilizes CFTR at the membrane by promoting its interaction with NHERF1**

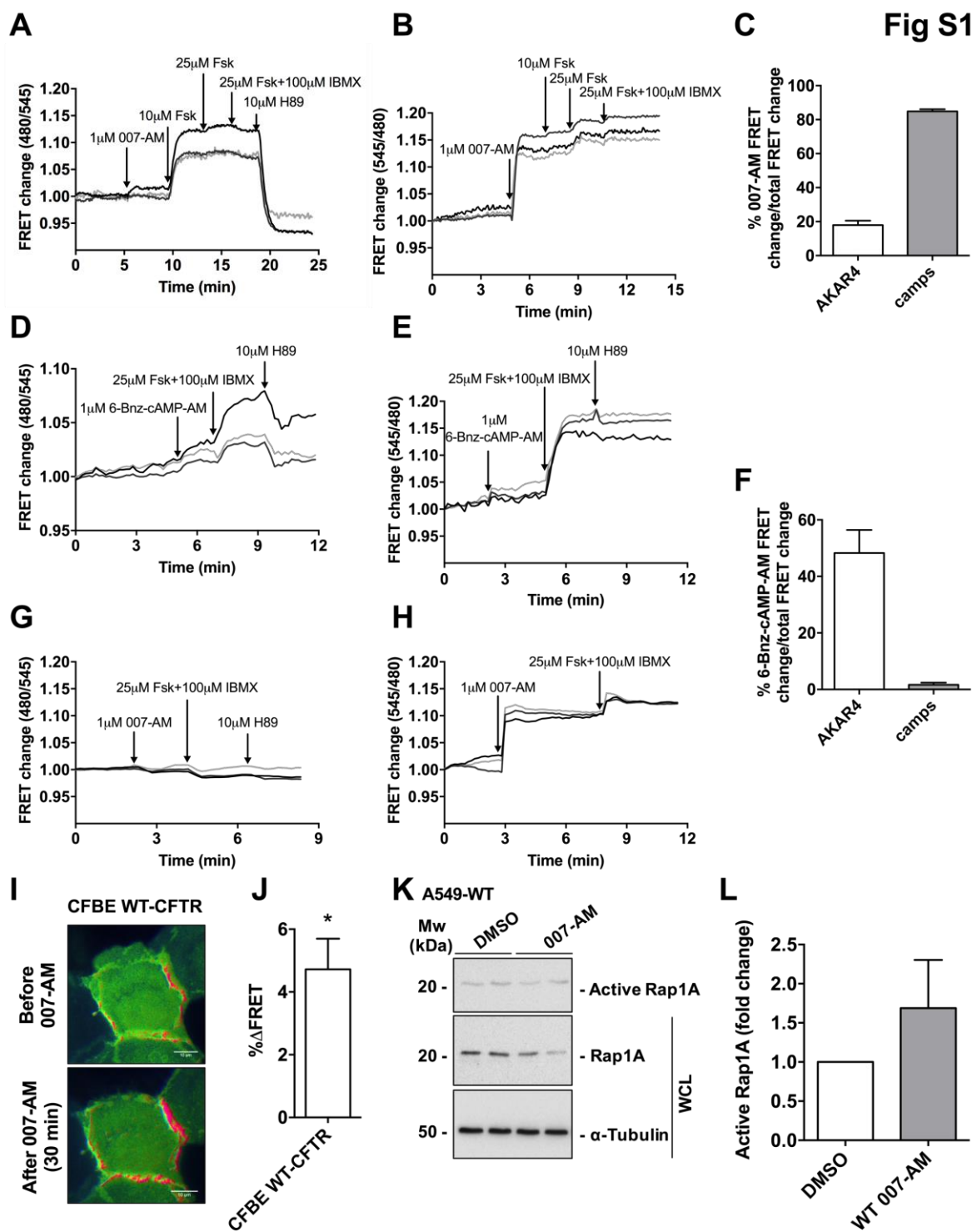
Miguel J Lobo, Margarida D Amaral, Manuela Zaccolo, Carlos M Farinha

**Figure S1**

**Figure S2**

**Figure S3**

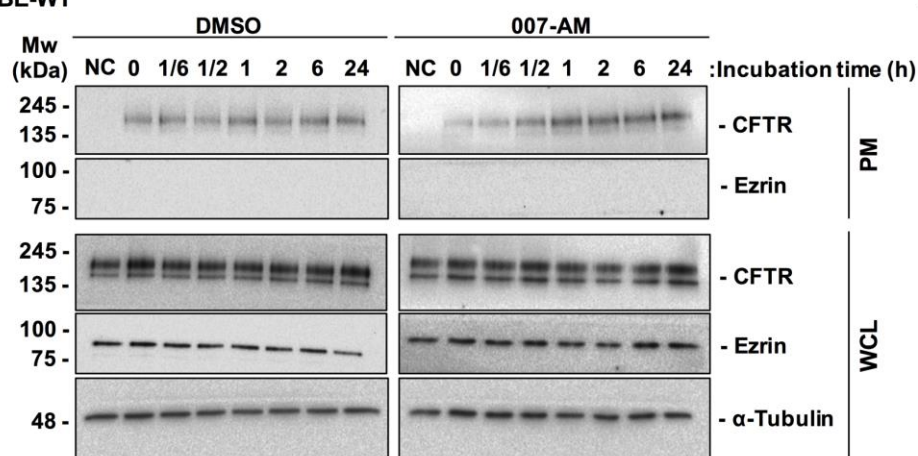
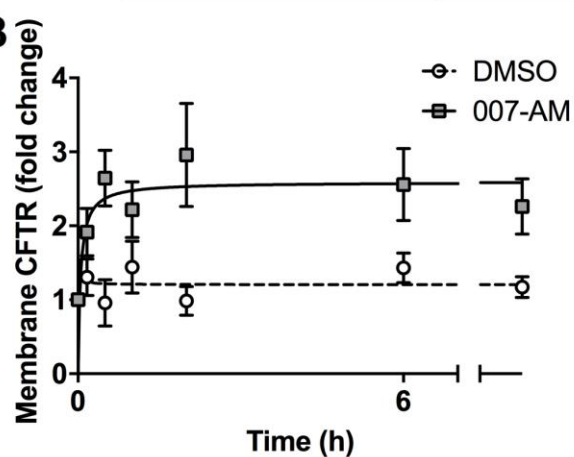
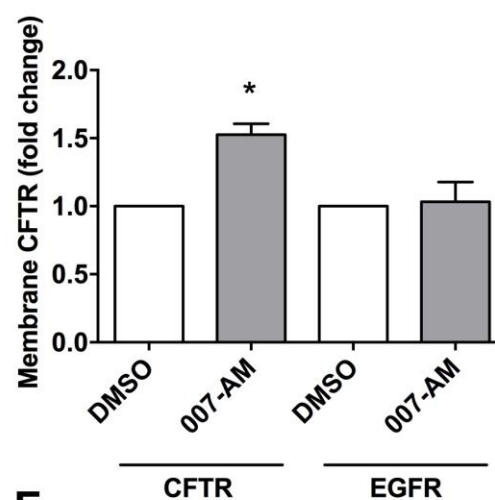
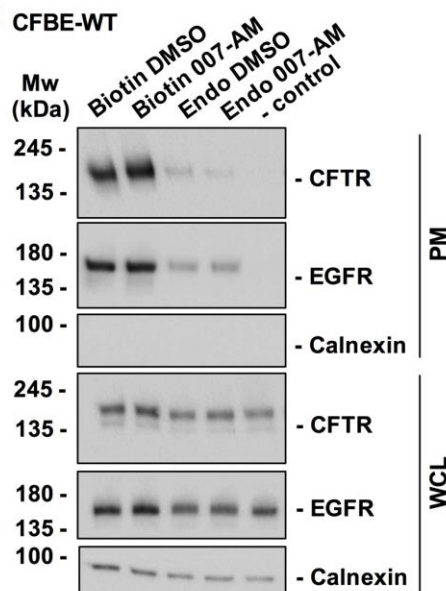
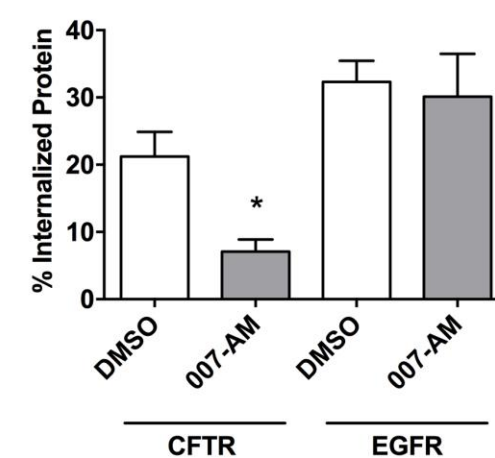
**Figure S4**



**Figure S1: cAMP-dependent activation of EPAC1 and PKA in CFBE cells.** FRET signal from (A) PKA activity-sensor AKAR4 and the (B) cAMP-sensor based on EPAC1 (camps) upon stimulation with 1  $\mu$ M 007-AM followed by increasing concentrations of Fsk. 25uM Fsk + 100uM IBMX represents a saturating condition where adenylate cyclases are fully activated and PDEs are inhibited, leading to higher levels of cAMP. H89, a PKA inhibitor, was used to show that the FRET change is due to a change in PKA activity. FRET change is the normalized 545nm/480nm or 480nm/545nm value calculated at each acquisition time point. The three lanes of each plot represent 3 different and independent cells. (C) Summary of all experiments performed in A and B, showing the percentage of 007-AM-induced FRET change compared to the maximum FRET change for both sensors. Data represent mean  $\pm$  SEM. n = 30/19 cells, 9/6 experiments (AKAR4/camps). FRET signal from (D) AKAR4 and (E) camps upon stimulation with 1  $\mu$ M 6-Bnz-cAMP-AM followed by 25uM Fsk + 100uM IBMX and then 10uM H89. The three lanes of each plot represent 3 different and independent cells. (F) Summary of all experiments performed in D and E, showing the percentage of 6-Bnz-cAMP-AM-induced FRET change compared to the maximum FRET change for both sensors. Data represent mean  $\pm$  SEM. n = 11/18 cells, 5/5 experiments (AKAR4/camps). FRET signal from (G) AKAR4 and (H) camps upon stimulation with 1  $\mu$ M 007-AM followed by 25uM Fsk + 100uM IBMX. The three lanes of each plot represent 3 different and independent cells. (I) EPAC1 activation after treatment with 007-AM. Analysis of Raichu-Rap FRET sensor upon stimulation of CFBE cells expressing wt-CFTR with 1 $\mu$ M 007-AM. Intensity-modulated pseudo-color images are shown here. Images show FRET signal before (upper panel) and 30 min after addition of 1 $\mu$ M 007-AM (lower panel). Scale bars, 10  $\mu$ m. (J) % $\Delta$ FRET represents the fold increase of the FRET signal at the PM (as a percentage) 30 min after the addition of 007-AM relative to pre-stimulus levels. \* means that the FRET signal after addition of 007-AM is significantly different compared to pre-stimulus condition ( $p < 0.05$ ). Data represent mean  $\pm$

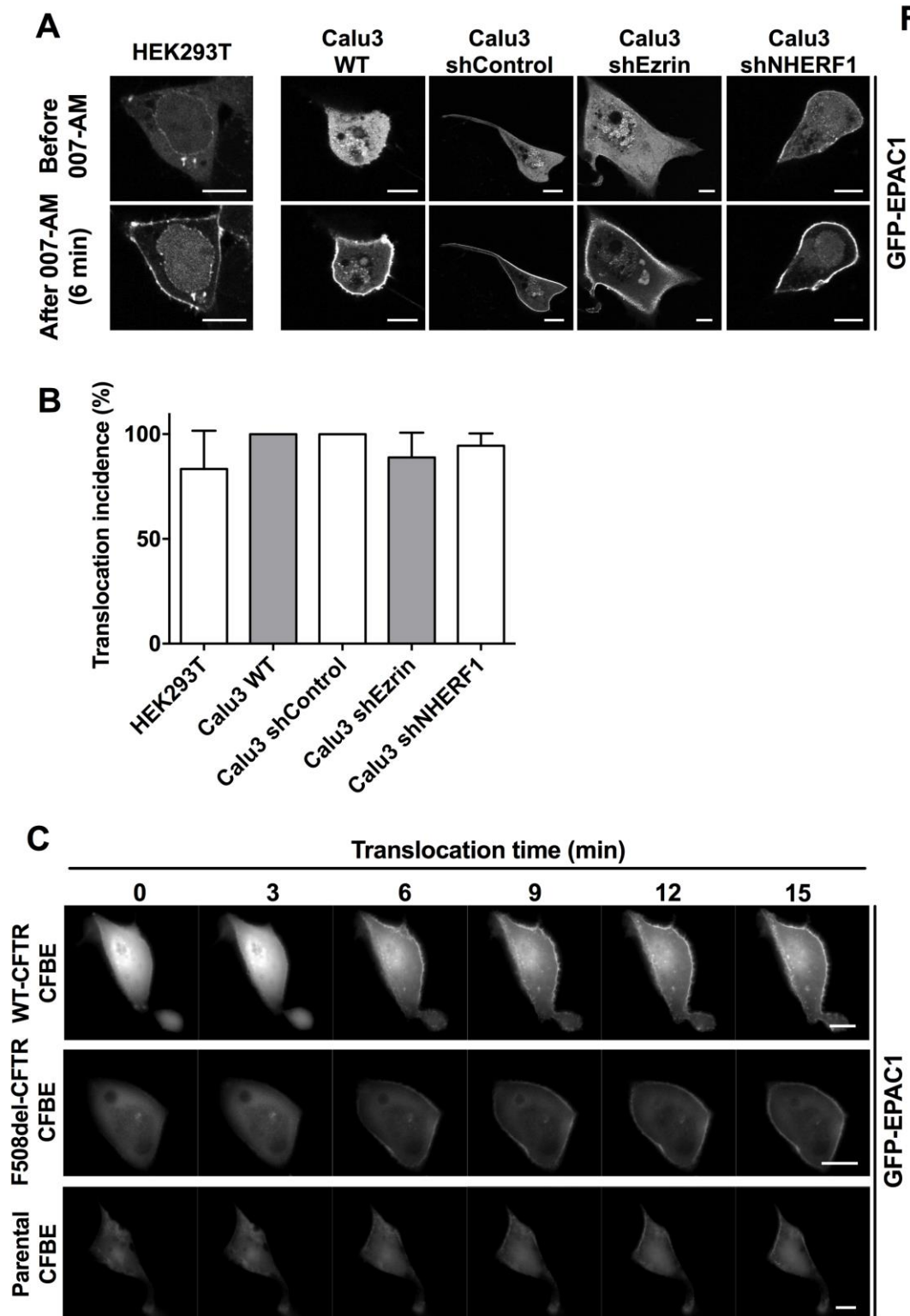
SEM. n = 28 cells, 13 experiments. **(K)** Western Blot showing the effect of 007-AM treatment upon the fraction of active Rap1A (using a specific pull-down assay – see Materials and Methods), in A549 cells expressing wt-CFTR. Cells were incubated with 1 $\mu$ M 007-AM for 2h (or DMSO as control). **(L)** Fold increase of active Rap1A after treatment with 007-AM for A549 cells expressing wt-CFTR. Amount of active Rap1A was normalized to the amount of total Rap1A and shown as fold change relatively to DMSO incubated cells. Data represent mean  $\pm$  SEM (n=4).

Fig S2

**A** CFBE-WT**B****D****C** CFBE-WT**E**

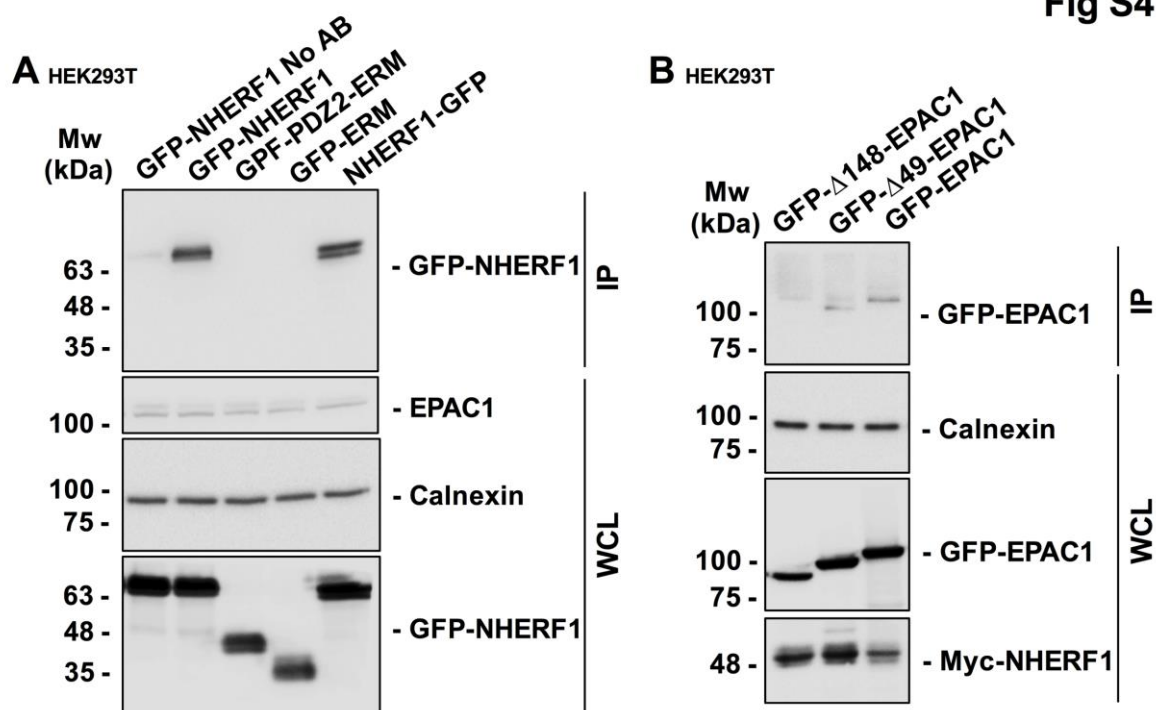
**Figure S2: CFTR and EGFR surface expression and endocytosis under EPAC1 activation.** (A) Time-course of CFTR plasma membrane levels under EPAC1 activation with 007-AM. CFBE-wt cells were treated with 1  $\mu$ M 007-AM for different time periods. After cell surface biotinylation and streptavidin pull-down, CFTR levels were assessed by WB. Samples not treated with biotin were considered as a negative control (NC). (B) Quantification of the amount of CFTR at the PM. Amount of CFTR at the PM was normalized to the amount of total CFTR and shown as fold change relatively to 0h. Data represent mean  $\pm$  SEM. n=3/4. (C) CFBE cells expressing wt-CFTR treated with 1 $\mu$ M 007-AM for 2h (or DMSO as control) were subjected to cell surface biotinylation, followed by incubation at 37°C (for 10 minutes). After that, cells were treated with a GSH solution and, after cell lysis and streptavidin pull-down, CFTR and EGFR were detected by WB. Samples not treated with GSH were considered as a positive control (Biotin). Samples not incubated at 37°C were considered as a negative control. (D) Quantification of the amount of CFTR/EGFR at the PM. Amount of CFTR/EGFR at the PM was normalized to the amount of total CFTR/EGFR and shown as fold change relatively to DMSO. Data represent mean  $\pm$  SEM (n=5-9). (E) Quantification of internalized CFTR/EGFR. The negative (-) control was subtracted from the amount of endocytosed CFTR/EGFR and values were normalized to the positive control (Biotin). Data represent mean  $\pm$  SEM (n=5-7).

Fig S3



**Figure S3: EPAC1 localization in HEK293, Calu3 and CFBE cells.** (A) Confocal live cell imaging analysis of GFP-EPAC1 localization in HEK293 and Calu3 cells. Images show EPAC1 staining before (upper panel) and 6 min after addition of 1 $\mu$ M 007-AM (lower panel). Scale bar 10  $\mu$ m. (B) The bar graph shows the percentage of cells showing translocation of EPAC1 to the PM upon 007-AM stimulation (Consonni et al., 2012) (n=9-19 cells, 6-11 experiments). (C) Live cell imaging of GFP-EPAC1 localization in CFBE parental, CFBE-wt and CFBE-F508del cells. Images were acquired every 3 min with 1 $\mu$ M 007-AM added after the acquisition at minute 3. Scale bar 10  $\mu$ m.

Fig S4



**Figure S4: Model for CFTR-EPAC1 interaction.** (A) Interaction of EPAC1 and NHERF1. Detection of NHERF1 deletion variants after immunoprecipitation of endogenously expressed EPAC1 in transiently transfected HEK293 cells. Pull-down with beads only (without conjugated antibody) was used as a negative control. GFP-NHERF1 and NHERF1-GFP have the GFP tag on either the N- or the C-terminus, respectively. GFP-PDZ2-ERM construct lacks PDZ1 domain while GFP-ERM construct lacks both PDZ1 and 2 domains. (B) Detection of EPAC1 deletion variants after immunoprecipitation of myc-NHERF1 in transiently transfected HEK293 cells. GFP- $\Delta$ 49-EPAC1 and GFP- $\Delta$ 148-EPAC1 lack the first 49 or 148 amino acids, respectively, of their N-terminal region.